OPEN ACCESS

Theoretical Insights into Equilibrium Potentials in Electrochemical Cells with Multiple Mobile Charge Carriers

To cite this article: Felix Ehrlich *et al* 2025 *J. Electrochem. Soc.* **172** 124521

View the article online for updates and enhancements.

You may also like

- Resolving a Discrepancy in Diffusion Potentials, with a Case Study for Li-Ion Batteries
Adrien M. Bizeray, David A. Howey and Charles W. Monroe
- Reversible SOFC Model as a Base of Design and Testing
Wolfgang Winkler
- Electrochemical Measurements on Cells. I: Simulation of Potential Distribution with an Embedded Probe
Lei Zhang, Feng Liu and Anil V, Virkar

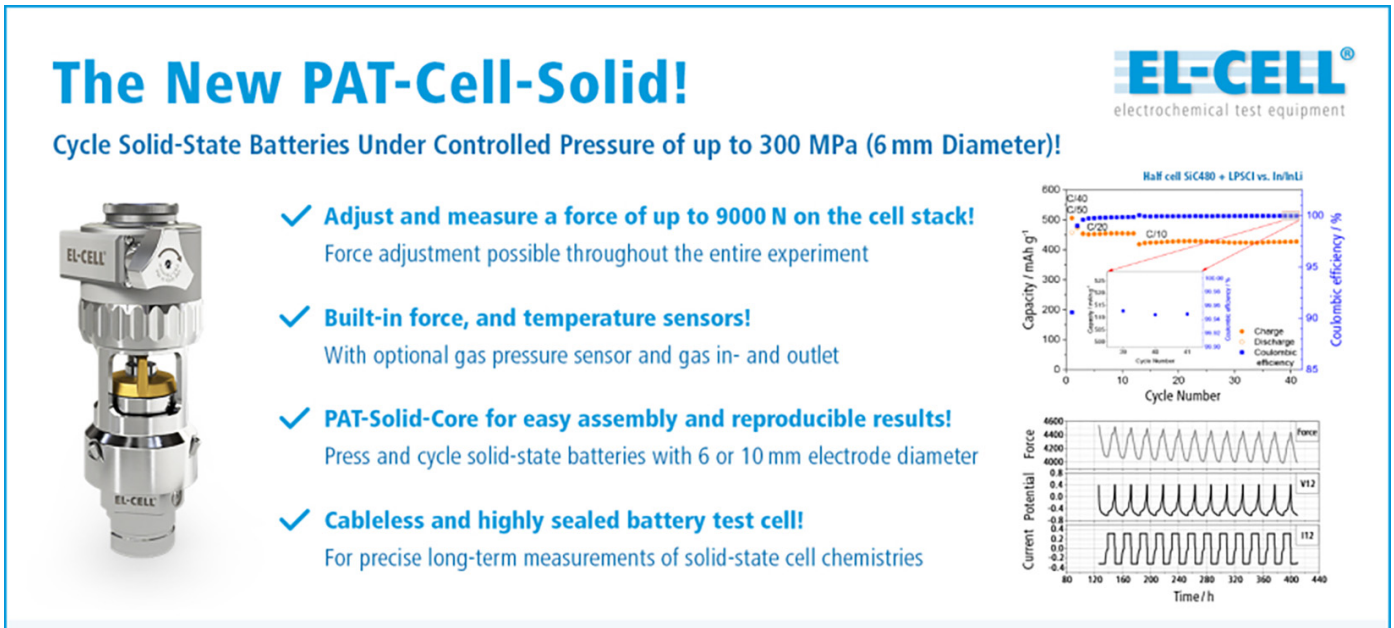

Journal of The Electrochemical Society, 2025 **172** 124521

Theoretical Insights into Equilibrium Potentials in Electrochemical Cells with Multiple Mobile Charge Carriers

Felix Ehrlich,[1] Akhil Ashar,[2] Oscar Furst,[1] Philipp Blanck,[1] Huayang Zhu,[2] Robert J. Braun,[2] Robert J. Kee,[2] and Olaf Deutschmann[1,z]

[1]*Institute for Chemical Technology and Polymer Chemistry (ITCP), Karlsruhe Institute of Technology, 76131 Karlsruhe, Germany*
[2]*Department of Mechanical Engineering, Colorado School of Mines, Golden, CO 80401, United States of America*

Equilibrium potentials are fundamental in electrochemistry, as they quantify the relation between chemical and electrostatic driving forces. For cells with multiple mobile charge carriers in the electrolyte—including those associated with electronic leakage—the calculation of equilibrium potentials is more complex than for cells with only one charge carrier, leading to inconsistent formulations in literature. The objective of this paper is to provide a theoretical framework for understanding and calculating equilibrium potentials in such cells, exemplified by the case of protonic ceramic cells. The analysis shows that reversible cell potentials cannot be predicted by Nernst equations based solely on the gas phase and instead require consideration of thermodynamic properties of the electrolyte. The impact of thermodynamically non-equilibrated inlet gases (like mixed fuels) on potentials in cells with multiple mobile charge carriers is investigated by use of mixed-potential theory. Finally, a distinction is made between reversible and measurable cell potential at open circuit, exemplified with BCZYYb-based cell simulations. Further analysis shows the potential difference is caused by overpotentials in electrodes and membrane. A theoretical scenario in which electronic leakage is prohibited reveals that the mere presence of multiple mobile charged defects causes differences between measurable and reversible cell potentials.

 [DOI: 10.1149/1945-7111/ae2959]

Manuscript submitted August 28, 2025; revised manuscript received November 18, 2025. Published December 23, 2025.

Nomenclature

a_k	Activity of species k
β_a, β_c	Anodic and cathodic CT symmetry factors
D_k	Diffusion coefficient of defect k
D_k°	Diffusion coefficient pre-exponential factor
E, $(\hat{E})$	(Shifted) potential difference between ed and el
$E_{\mathrm{act},k}$	Diffusion coefficient activation energy of species k
E_{act}^r	Activation energy of exchange current density from CT reaction r
E^{eq}, $(\hat{E}^{\mathrm{eq}})$	(Shifted) equilibrium potential of half cell
$E^{\mathrm{eq},r}$, $(\hat{E}^{\mathrm{eq},r})$	(Shifted) equilibrium potential of CT reaction r
$E^{\mathrm{eq,ref}}$	Half cell reference equilibrium potential
E^{mix}, $(\hat{E}^{\mathrm{mix}})$	(Shifted) mixed half cell potential at steady-state
ΔE^{mix}	Cell potential containing a mixed half cell potential at steady-state
$E_{\mathrm{Nernst(gas)}}^r$	Gas-phase based Nernst potential contribution from cell reaction r
$E_{\mathrm{Nernst(def.)}}^r$	Defect-based based Nernst potential contribution from cell reaction r
E_{OCV}	Open-circuit voltage
E_{rev}	Equilibrium cell potential
η^r	Overpotential for CT reaction r
F	Faraday constant
$\Delta_r\widetilde{G}$	Molar electrochemical reaction Gibbs energy
$\Delta_r G$	Molar chemical reaction Gibbs energy
$\Delta_r G^\circ$	Molar standard chemical reaction Gibbs energy
γ	Reference shift of electrolyte potential
i^r	Charge transfer rate of reaction r
$i^{0,r}$	Exchange current density of reaction r
$i_0^{0,r}$	Pre-factor of exchange current density from CT reaction r
J_k	Defect flux of species k
k	Species index
$K_{\mathrm{ads},k}$	Equilibrium constant for adsorption of gas species k on Ni surface
$K_{p,r}$	Equilibrium constant of reaction r
$\widetilde{\mu}_k$	Electrochemical potential of species k
μ_k	Chemical potential of species k
μ_k°	Standard state chemical potential of species k
ν_k	Stochiometric coefficient (positive and negative) of species k
p_k	Partial pressure of species k
p°	Standard pressure
Φ_{ed}	Electrostatic potential in electrically conductive phase
Φ_{el}, $(\hat{\Phi}_{\mathrm{el}})$	(Shifted) electrostatic potential in electrolyte phase
$\dot{q}_r$	Reaction rate of reaction r
R	Ideal gas constant
r	Reaction index
$\mathbf{R}_{\mathrm{CT}}$	All CT reactions present in the system
$\mathbf{S}_{\mathrm{el}}$	All electrolyte species present in the electrolyte material
$\mathbf{S}_r$	All species participating in reaction r
$\dot{s}_k$	Formation rate of species k
σ_k	Conductivity of species k
t_k	Transference number of species k
V_{m}	Molar volume of bulk electrolyte
x_k	Mole fraction of species k
z_k	Charge of species k
z_r	Electrons produced in reaction r (anodic direction)
$\mathrm{h}^\bullet$	Electron hole
$\mathrm{O}_{\mathrm{O}}^\bullet$	Polaron
$\mathrm{OH}_{\mathrm{O}}^\bullet$	Proton
$\mathrm{O}_{\mathrm{O}}^{\mathrm{x}}$	Lattice oxygen
$\mathrm{V}_{\mathrm{O}}^{\bullet\bullet}$	Lattice oxygen vacancy
$\mathrm{X}_{\mathrm{B}}^{\prime}$	Combined dopants

In fuel cells, electrolyzers, batteries, and other electrochemical devices, equilibrium potentials are of interest as they are related to the Gibbs energy and thus the reversible work associated with the electrochemical processes.[1–3] Further, equilibrium potentials are used to determine overpotentials and evaluate cell voltage efficiency, which is an integral part of the overall cell energy efficiency.[4–6] In potentiometric sensors on the other hand, measured equilibrium potentials enable concentration quantification for electrochemically

[z]E-mail: deutschmann@kit.edu

active species.[7,8] In experimental studies, equilibrium potentials are commonly used as references for comparing measured open-circuit voltages, providing, for example, qualitative assessments on gas tightness and membrane integrity in manufactured cells.[9,10] In electrochemical models, equilibrium potentials are required to correctly represent the thermodynamic driving forces for electrochemical processs, and are thus fundamental for achieving thermodynamically accurate predictions. A correct quantification of equilibrium potentials is therefore quite important in electrochemical research. The work presented here discusses reversible cell potentials, mixed cell potentials and the measurable open-circuit voltage in the context of cells with multiple mobile charge carriers.

Electrochemical equilibrium potentials are established when the charge-transfer (CT) reactions in forward and reverse directions proceed at equal rates.[11] When electrochemical reactions involve CT across electrode-electrolyte phases, an electrostatic equilibrium potential is formed across these phases.[2] In many electrochemical cells, an electrolyte membrane separates the two half cells where electrochemical reactions occur. The electrolyte participates in the CT reactions and enables the transport of mobile charge carriers such as protons $OH_O^{\bullet}$ (Kröger-Vink notation) or oxygen lattice vacancies ($V_O^{\bullet\bullet}$) between electrodes, thus closing the mass and charge balance between reactions. Based on the particular mobile charge carriers in the electrolyte, different CT reactions can influence the cell's equilibrium potentials. For example, if the electrolyte is capable of conducting only one type of mobile charge carrier at significant rates it is classified as single charged defect conductor (SCDC). If an SCDC such as Yttria Stabilized Zirconia (YSZ), which conducts $V_O^{\bullet\bullet}$, separates H_2 from air, two half-cell CT reactions are possible—the H_2-vacancy-charge-transfer (HVCT) in the negatrode

$$H_2(g) + O_O^{x}(el) \rightleftharpoons V_O^{\bullet\bullet}(el) + H_2O(g) + 2\,e'(ed) \quad [1]$$

and the O_2-vacancy-charge-transfer (OVCT) in the positrode

$$O_O^{x}(el) \rightleftharpoons 0.5\,O_2(g) + V_O^{\bullet\bullet}(el) + 2\,e'(ed). \quad [2]$$

Together, these two reactions combine to represent a vacancy-based cell reaction (VCR)

$$H_2(g,\,nt) + 0.5\,O_2(g,\,pt) \overset{V_O^{\bullet\bullet}}{\rightleftharpoons} H_2O(g,\,nt). \quad [3]$$

The parenthetical (g) refers to gas phase, (el) to the electrolyte phase and (ed) to the electron-conducting phase. The parenthetical (nt) represents the negatrode and (pt) the positrode. The electrostatic equilibrium potential at which all reactions are thermodynamically equilibrated is the reversible cell potential. Based on a particular VCR, the reversible cell potential in an SCDC-based symmetrical cell can be quantified through a gas-phase-based Nernst equation[12–15] as

$$E^{\mathrm{V\,CR}}_{\mathrm{Nernst(gas)}} = -\frac{\Delta_r G^{\circ}_{\mathrm{WFR}}(T)}{2F} + \frac{RT}{2F}\ln\left(\frac{p_{\mathrm{H_2,nt}}\,(p_{\mathrm{O_2,pt}})^{1/2}}{p_{\mathrm{H_2O,nt}}\,(p^{\circ})^{1/2}}\right), \quad [4]$$

where R is the gas constant, F the Faraday constant, p_k the partial pressure of the gas species k and p° the standard-state pressure. $\Delta_r G^{\circ}_{\mathrm{WFR}}(T)$ is the standard molar formation enthalpy of water according to the gas-phase water-formation reaction (WFR):

$$H_2(g) + 0.5\,O_2(g) \rightleftharpoons H_2O(g). \quad [5]$$

Notably, the VCR (Eq. 3) produces H_2O within the negatrode, as $V_O^{\bullet\bullet}$ is responsible for charge transport through the membrane electrode assembly (MEA).

Compared to SCDC, electrolyte materials with multiple mobile charge carrier (MCDC) electrolytes may allow for more charge transfer reactions. For example, BCZYYb ($BaCe_{0.7}Zr_{0.1}Y_{0.1}Yb_{0.1}O_{3-\delta}$), which is frequently used in protonic-ceramic cells (PCCs), is capable of conducting protons $OH_O^{\bullet}$ and oxygen vacancies $V_O^{\bullet\bullet}$ as well as small polarons $O_O^{\bullet}$.[16] Small polarons are charge carriers associated with electronic leakage currents, making BCZYYb a mixed ionic-electronic conductor (MIEC).[16]

The reversible cell potential in cells with multiple mobile charge carriers (the usual case for PCCs) is frequently represented using a purely gas-phase-based Nernst equation,[17–21] such as

$$E^{\mathrm{HCR}}_{\mathrm{Nernst(gas)}} = -\frac{\Delta_r G^{\circ}_{\mathrm{WFR}}(T)}{2F} + \frac{RT}{2F}\ln\left(\frac{p_{\mathrm{H_2,nt}}\,(p_{\mathrm{O_2,pt}})^{1/2}}{p_{\mathrm{H_2O,pt}}\,(p^{\circ})^{1/2}}\right), \quad [6]$$

originating from the proton-based cell reaction (HCR)

$$H_2(g,\,nt) + 0.5\,O_2(g,\,pt) \overset{OH_O^{\bullet}}{\rightleftharpoons} H_2O(g,\,pt). \quad [7]$$

This formulation results from two half-cell charge-transfer reactions. At the negatrode the H_2-proton-charge-transfer (HHCT) may be represented as

$$H_2(g) + 2\,O_O^{x}(el) \rightleftharpoons 2\,OH_O^{\bullet}(el) + 2\,e'(ed), \quad [8]$$

and the O_2-proton-charge-transfer (OHCT) at the positrode as

$$2\,O_O^{x}(el) + H_2O(g) \rightleftharpoons 0.5\,O_2(g) + 2\,OH_O^{\bullet}(el) + 2\,e'(ed). \quad [9]$$

The proton-based charge transport through the MEA leads to H_2O production in the positrode. While sometimes a reasonable approximation of the reversible cell potential in PCCs, the Nernst potential $E^{\mathrm{HCR}}_{\mathrm{Nernst(gas)}}$ neglects the ability of many protonic-ceramic electrolytes to conduct both $OH_O^{\bullet}$ and $V_O^{\bullet\bullet}$.[22] This enables both cell reactions HCR and VCR, suggesting simultaneous applicability of both Nernst potentials $E^{\mathrm{HCR}}_{\mathrm{Nernst(gas)}}$ and $E^{\mathrm{V\,CR}}_{\mathrm{Nernst(gas)}}$ in PCCs. Importantly, the two gas-phase-based Nernst equations lead to different cell potentials. As such, the difference between the two representations corresponds to the difference in steam partial pressure across the MEA:

$$E^{\mathrm{V\,CR}}_{\mathrm{Nernst(gas)}} - E^{\mathrm{HCR}}_{\mathrm{Nernst(gas)}} = \frac{RT}{2F}\ln\left(\frac{p_{\mathrm{H_2O,pt}}}{p_{\mathrm{H_2O,nt}}}\right). \quad [10]$$

The disparity between equations $E^{\mathrm{HCR}}_{\mathrm{Nernst(gas)}}$ and $E^{\mathrm{V\,CR}}_{\mathrm{Nernst(gas)}}$ illustrates the principal problem of using purely gas-phase-based Nernst equations to predict the reversible cell potential in MCDC cells, as they do not consider cell potential contributions originating from mobile defect concentration differences between electrodes. The ambiguity of the two supposedly equally applicable gas-phase based Nernst equations for PCCs has been reported previously, but was not fully resolved with respect to thermodynamic equilibrium.[23] This possibly explains why some studies evaluate reversible cell potentials only for the case of equal humidities in both electrodes (e.g.,[24]).

The present analysis develops a Nernst equation that is appropriate for evaluating the reversible cell potential in cells with multiple mobile charge carriers. It considers the influence of non-electrochemical side reactions and closes the energy gap between $E^{\mathrm{V\,CR}}_{\mathrm{Nernst(gas)}}$ and $E^{\mathrm{HCR}}_{\mathrm{Nernst(gas)}}$. Its calculation considers all information necessary to unambiguously define the chemical potentials of all mobile charge carriers in each half cell—a condition that is not fulfilled by either Eq. 4 or Eq. 6. The approach is based on previous publications from Zhu et al.,[25–28] and applied to PCCs leads to equations in accordance with prior literature.[29,30]

The present analysis considers the behaviors of competing charge-transfer reactions and equilibrium potentials in the presence of equilibrated and non-equilibrated gas compositions. Examples where simultaneous charge transfer may occur include PCC membranes for the electrochemical production of H_2 via electrolysis,[31,32] NH_3 production from N_2,[33,34] and CH_4 synthesis from CO_2 reduction.[35–37] Mixed-potential theory is needed to calculate the

equivalent of a reversible cell potential in the case of a non-equilibrated gas phase.

In PCCs the electrostatic potential measured under open-circuit conditions (i.e., the open-circuit voltage OCV) is lower than the reversible cell potential. This deviation is typically attributed to electronic leakage through the membrane. Typical analytical approaches, which are limited to reversible electrodes, quantify the potential drop using transference numbers of mobile charge carriers.[38–42] In the present work, a one-dimensional button-cell model is used to analyze the impact of the leakage currents on the electrostatic-potential profiles throughout the MEA, while considering non-reversible electrodes, and thus accommodating spatially distributed contributions to the potential drop. The results show that the presence of multiple mobile defects, without charge carriers associated with electronic leakage, also lead to a deviation between measured and theoretical potentials—a fact frequently neglected when explaining the reduced OCV in PCCs.[19,43–46]

While here PCCs are used as an example, the presented procedures for deriving reversible, mixed and and measured cell potentials are general. They broadly apply to different ceramics or cell types (e.g., cells based on SCDCs such as YSZ, MIECs such as gadolinium-doped ceria, or potentiometric sensor configurations measuring mixed or equilibrium potentials).

Equilibrium Potentials

The present Section considers equilibrium potentials in systems with multiple mobile charge carriers. The Section highlights the relationships among equilibrium potentials associated with individual charge-transfer reactions in the presence of thermodynamically equilibrated and non-equilibrated gas compositions. The analysis also considers the influence of non-electrochemical side reactions and the consequences for the equilibrium potential of the entire cell.

Equilibrium potential from thermodynamics.—This Section presents a general approach to evaluate charge-transfer, half-cell, and full-cell equilibrium potentials from thermodynamics, regardless of the electrolyte material. The overall cell reaction is a the result of individual CT processes taking place in the contributing half cells. The analysis assumes that each half cell is composed of three phases. First, a porous electrolyte phase (el) that is responsible for defect charge transport (represented in green in Figure 1). Second, an electron-conducting electrode phase (ed) that enables electron uptake and donation (represented in gray). Third, a reactive gas phase (g) that occupies the pore volume. Assume further that the electrolyte phase and the electrode phase are the same material in both composite electrodes. This assumption avoids the possibility of interfacial potential differences and space-charge layers at electrolyte-electrolyte heterointerfaces, which are beyond the scope of the present work, but are discussed elsewhere.[47–50]

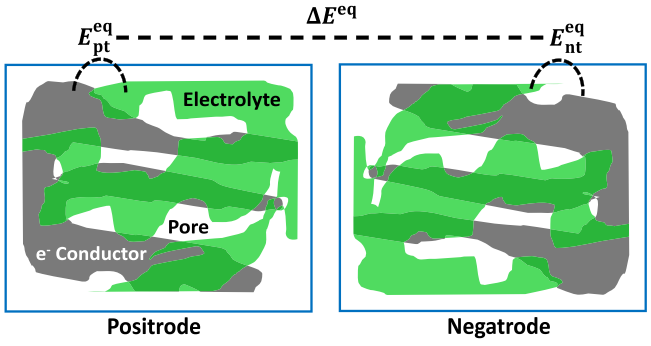

Figure 1. Separated half cells consisting of an ionic electrolyte, electron-conducting electrode phase, and a pore structure. There is no dense electrolyte membrane connecting the half cells.

Half-cell equilibrium potentials ensure the equilibration of each charge-transfer reaction in the respective half cell. Further, the evaluation of half-cell equilibrium potentials has to disregard the influence of a dense electrolyte membrane between the two half-cells, as shown in Figure 1, since defect transport through the membrane, such as leakage currents and charged-defect flux, can induce non-equilibrium conditions for electrolyte membranes with multiple mobile charge carriers, thereby invalidating the assumptions required to define thermodynamic equilibrium potentials.

Half-cell charge-transfer reactions typically occur at triple-phase boundaries that are formed at the intersections between electrolyte, electrode, and gas phases. A generic reaction r may be expressed as

$$n_1\,\mathrm{R_1(g)} + \mathrm{n_2\,R_2^{z_2}(el)} \rightleftharpoons n_3\,\mathrm{P_3^{z_3}(el)} + \mathrm{n_4\,e^{z_4}(ed)}, \qquad [11]$$

where R_k and P_k represent reactants and products, respectively. The variables n_k are stoichiometric coefficients of participating species k and the parameters z_k are the species charge relative to a perfect ceramic O^{-2} lattice (e.g., for a proton $z_{\mathrm{OH_O^\bullet}} = +1$). Each species has an electrochemical potential $\widetilde{\mu}_k(T)$, which may be expressed as

$$\widetilde{\mu}_k(T) = \underbrace{\mu_k^\circ(T) + RT\,\ln(a_k)}_{\mu_k(T)} + z_k F \Phi_k, \qquad [12]$$

where $\mu_k(T)$ is the chemical potential, $\mu_k^\circ(T)$ is the standard-state chemical potential. The variable Φ_k is the electrostatic potential of the phase in which species k resides, assuming that the species adopts the potential of its surrounding phase.[51] The gas phase is considered to be electrically neutral.[52] The variables a_k are the activities, which, for an ideal solution, can be approximated by the species concentration according to $a_k = [\mathrm{X}_k]/c^\circ$ for condensed-phase species (solids or liquids), or the partial pressures for gases as $a_k = p_k/p^\circ$. Here, c° and p° have the numerical value of unity and the unit based on the reference chosen in the definition of $\mu_k^\circ(T)$. The activity of electrons in pure metals is unity.[53] If the charge-transfer reaction r is equilibrated, the molar *electrochemical* reaction Gibbs energy $\Delta_r\widetilde{G}(T)$ is zero.[54] Expressed mathematically,

$$\begin{aligned}\Delta_r\widetilde{G}(T) &= \sum_{k\,\in\,\mathbf{S}_r} \nu_k \widetilde{\mu}_k(T) \\ &= \underbrace{\sum\nolimits_{k\,\in\,\mathbf{S}_r} \nu_k \mu_k(T)}_{\Delta_r G(T)} + \sum_{k\,\in\,\mathbf{S}_r} \nu_k z_k F \Phi_k = 0,\end{aligned} \qquad [13]$$

with $\nu_k = -n_k$ for reactants (i.e., ν_k is negative for reactants) and $\nu_k = n_k$ for products from reaction (11). The vector $\mathbf{S}_r$ represents all species participating in reaction r. $\Delta_r G(T)$ is the molar *chemical* reaction Gibbs energy. For every electrically neutral species the electrochemical and chemical potentials are identical (i.e., $\widetilde{\mu}_k(T) = \mu_k(T)$) because $z_k = 0$. Similarly, if a reaction does not include the transfer of an electron *between* phases, the electrochemical and the chemical-reaction Gibbs energies are identical (i.e., $\Delta_r G(T) = \Delta_r\widetilde{G}(T)$) because the second summation containing Φ_k vanishes. An equilibrium potential $E^{\mathrm{eq},r}$ for the half-cell CT reaction r can be defined as[25,26,52,55]

$$E^{\mathrm{eq},r} = \Phi_{\mathrm{ed}}^{\mathrm{eq},r} - \Phi_{\mathrm{el}}^{\mathrm{eq},r}, \qquad [14]$$

where $\Phi_{\mathrm{ed}}^{\mathrm{eq},r}$ and $\Phi_{\mathrm{el}}^{\mathrm{eq},r}$ are the equilibrium electrostatic potentials for the electrode and electrolyte phases, respectively.

Equation 13 can be expressed alternatively, resulting in the Nernst equation for a single interface, which is also in accordance with mass-action-law-based derivations[11] as

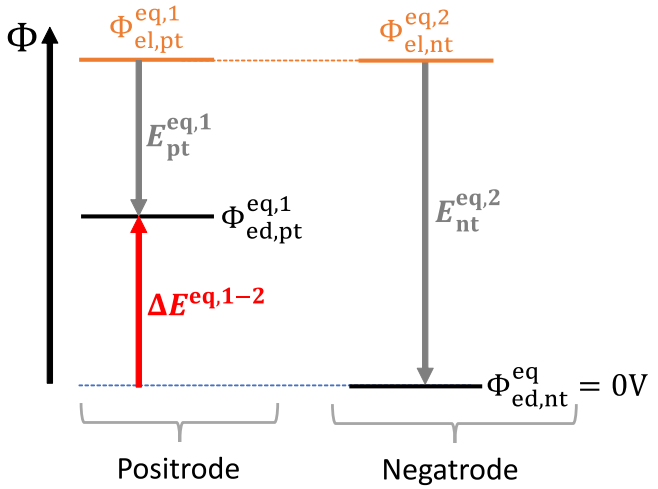

Figure 2. Electrostatic potentials in two half cells with one CT reaction each and a shared electrolyte potential chosen as common reference.

$$E^{eq,r} = -\frac{\sum_k \nu_k z_k F \Phi_k}{z_r F} = \frac{\Delta_r G(T)}{z_r F} = \frac{\Delta_r G^\circ(T)}{z_r F} + \frac{RT}{z_r F} \ln\left(\prod_{k \in S_r} a_k^{\nu_k}\right), \quad [15]$$

where z_r is the number of electrons transferred per mole of species referenced in the definition of $\Delta_r \widetilde{G}(T)$ (i.e., $z_r = n_4$ for the generic reaction (11)). It is important to realize, that Eq. 15 includes the activities of mobile charge carriers produced or consumed by the charge transfer reaction. Using the general formulation of $E^{eq,r}$ (Eq. 15), Eq. 13 for equilibrated CT can be rewritten as

$$\Delta_r \widetilde{G}(T) = \Delta_r G(T) - z_r F E^{eq,r} = 0. \quad [16]$$

In this representation, $E^{eq,r}$ is the potential difference required for balancing the chemical potential difference $\Delta_r G(T)$, such that the reaction rate of half-cell CT reaction r vanishes (i.e., remains in equilibrium).

Figure 2 shows a potential diagram where the negatrode electric potential is used as the reference. It illustrates the potential difference $E^{eq,r}$ as gray arrows between the potential $\Phi^{eq,r}_{ed}$ in the electron-conducting phase and the potential $\Phi^{eq,r}_{el}$ in the electrolyte in two half cells, according to Eq. 14.

In the trivial case of a single CT reaction per half cell, charge-transfer and half-cell equilibrium potentials are identical. Using the definition of Eq. 14, the difference between two half-cell equilibrium potentials can be evaluated as[52]

$$\Delta E^{eq,1-2} = E^{eq,1}_{pt} - E^{eq,2}_{nt} = \Phi^{eq,1}_{ed,pt} - \Phi^{eq,1}_{el,pt} - (\Phi^{eq,2}_{ed,nt} - \Phi^{eq,2}_{el,nt}) = \underbrace{(\Phi^{eq,1}_{ed,pt} - \Phi^{eq,2}_{ed,nt})}_{\text{electronic}} + \underbrace{(\Phi^{eq,2}_{el,nt} - \Phi^{eq,1}_{el,pt})}_{\text{ionic}} = E_{rev}. \quad [17]$$

For a cell with only one CT reaction per half cell, the difference between both half-cell equilibrium potentials equals the reversible cell potential E_{rev}.[51] Equation 17 suggests that the total energy difference between the half cells is distributed across an electronic- and an ionic-potential difference. The distribution is arbitrary because there is no common electronic or ionic connection between the half cells. Thus, absolute potentials are unrelated across the half cells. A reference potential can be chosen by shifting all potentials in one half cell such that $\Phi^{eq,1}_{el,pt} = \Phi^{eq,2}_{el,nt}$. Figure 2 shows the (shifted) electrolyte potentials for two half cells in orange. With the common reference in mind, Eq. 17 can be reformulated as

$$\Delta E^{eq,1-2} = E^{eq,1}_{pt} - E^{eq,2}_{nt} = \underbrace{\Phi^{eq,1}_{ed,pt} - \Phi^{eq,2}_{ed,nt}}_{\text{electronic}} = E_{rev}. \quad [18]$$

The resulting reversible cell potential $\Delta E^{eq,1-2}$ is therefore the electrostatic potential difference between the electron conducting phases of each half cell, shown in Fig. 2 as a red arrow.

Reactions in PCCs.—Evaluating CT equilibrium potentials (Eq. 15), requires knowing the activities of all participating species. The species activities depend on the type of electrolyte material used, as well as on reactants. The present Section uses illustrative reactions for protonic-ceramic cells and explains how the reactions depend on thermodynamic parameters.

Protonic-ceramic cells consist of a porous composite negatrode (nt) contacting a reducing gas such as H_2, a dense electrolyte impermeable to gas transport, and a porous positrode (pt) in contact with an oxidant such as humid air or steam with some O_2 (cf., Fig. 3). The reducing atmosphere at the negatrode enables the utilization of a cermet (e.g., Ni-BCZYYb), ensuring electronic and ionic conductivity. The oxidative environment in the positrode prohibits the use of reduced metals for increased electron conduction, and instead requires an electrolyte with good electronic conductivity, such as $La_{0.6}Sr_{0.4}Co_{0.2}Fe_{0.8}O_{3-\delta}$ (LSCF). Protonic conductivity can be enhanced in the positrode by adding BCZYYb to LSCF.[56,57] The outer ends of the electrodes contact current collectors and an external electrical circuit enables electron transport between the electrodes (Fig. 3).

Acceptor-doped ABO_3 perovskites such as BCZYYb are among the most widely used electrolyte materials for PCCs.[58] The doping causes the formation of oxygen-lattice vacancies $V_O^{\bullet\bullet}$, as well as more mobile protons $OH_O^\bullet$ when exposing the ceramic to a humid gas environment.[22] Electronic conductivity in proton-conducting ceramics may originate from delocalized electrons (e'), delocalized electron holes ($h^\bullet$), and in case of cerium-containing materials such as BCZYYb also cerium reduction. In reducing environments the electronic conductivity of BCZYYb is low, suggesting that the contribution of e' and reduced cerium, which are likely to be produced in reducing environments, is negligible compared to the leakage currents associated with hole conduction.[16,59] Electron holes may be considered to be localized on lattice oxygen, thus being properly identified as small polarons ($O_O^\bullet$).[60–63] That is to say,

$$h^\bullet + O_O^x(el) \rightleftharpoons O_O^\bullet(el). \quad [19]$$

Exposure of the doped-ceramic electrolyte to humid hydrogen or humid oxygen leads to specific equilibrium concentrations of the mobile defects $OH_O^\bullet$, $V_O^{\bullet\bullet}$ and $O_O^\bullet$. The equilibration process proceeds by means of incorporation reactions. For example, hydrogen incorporation reaction (HIR) as

$$0.5\, H_2(g) + O_O^\bullet(el) \rightleftharpoons OH_O^\bullet(el), \quad [20]$$

oxygen incorporation reaction (OIR) as

$$0.5\, O_2(g) + O_O^x(el) + V_O^{\bullet\bullet}(el) \rightleftharpoons 2\, O_O^\bullet(el), \quad [21]$$

and water incorporation reaction (WIR) as

$$H_2O(g) + V_O^{\bullet\bullet}(el) + O_O^x(el) \rightleftharpoons 2\, OH_O^\bullet(el). \quad [22]$$

Equilibria of these reactions can be expressed through equilibrium constants K_p[64] as

$$K_{p,HIR} = \frac{[OH_O^\bullet]_L^{eq}}{(p_{H_2}^{eq})^{1/2} [O_O^\bullet]_L^{eq}}, \quad [23]$$

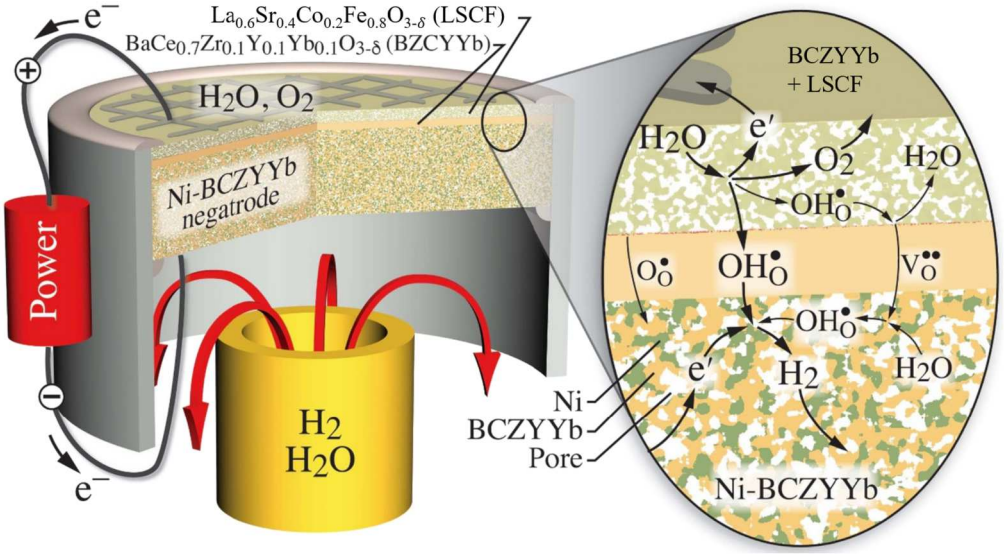

Figure 3. Illustration of a protonic ceramic electrolysis cell producing hydrogen and oxygen from steam, based on BCZYYb as electrolyte. CT reactions HHCT (8) and OHCT (9), as well as incorporation WIR (22) are depicted in the enlargement. Figure adapted from,[45] licensed under CC BY 4.0.

Table I. Thermodynamic parameters for BCZYYb defect chemistry.[16]

Reactions	$\Delta_r H^\circ$ [kJ/mol]	$\Delta_r S^\circ$ [J/(mol K)]	K_p @ 600 °C
$0.5\,H_2 + O_O^\bullet \rightleftharpoons OH_O^\bullet$	−180.80	−60.83	$4.36 \times 10^{+7}$
$0.5\,O_2 + O_O^x + V_O^{\bullet\bullet} \rightleftharpoons 2\,O_O^\bullet$	−16.50	−60.30	6.87×10^{-3}
$H_2O + V_O^{\bullet\bullet} + O_O^x \rightleftharpoons 2\,OH_O^\bullet$	−130.00	−126.47	$1.48 \times 10^{+1}$

$$K_{p,\mathrm{OIR}} = \frac{([O_O^\bullet]_L^{eq})^2}{(p_{O_2}^{eq})^{1/2}[O_O^x]_L^{eq}[V_O^{\bullet\bullet}]_L^{eq}}, \quad [24]$$

$$K_{p,\mathrm{WIR}} = \frac{([OH_O^\bullet]_L^{eq})^2}{p_{H_2O}^{eq}[O_O^x]_L^{eq}[V_O^{\bullet\bullet}]_L^{eq}}. \quad [25]$$

Thermodynamic parameters for the K_p values for BCZYYb have been reported by Zhu et al.[16] and are given in Table I.

A general expression for K_p may be stated as

$$K_p = \exp\left(-\frac{\Delta_r G^\circ}{RT}\right) = \exp\left(\frac{\Delta_r S^\circ}{R}\right)\exp\left(-\frac{\Delta_r H^\circ}{RT}\right) = \frac{k_f}{k_b}, \quad [26]$$

with k_f and k_b being incorporation forward and backward reaction rate constants. Note that the equilibrium of the WFR (Eq. 5) can be expressed as a linear combination of defect incorporation reactions HIR (Eq. 20), OIR (Eq. 21) and WIR (Eq. 22). Therefore, to ensure thermodynamic consistency, the incorporation equilibrium constants must also combine to the water formation equilibrium constant $K_{p,\mathrm{WFR}}$,

$$K_{p,\mathrm{HIR}}^2\, K_{p,\mathrm{OIR}} = K_{p,\mathrm{WIR}}\, K_{p,\mathrm{WFR}}, \quad [27]$$

with

$$K_{p,\mathrm{WFR}} = \frac{p_{H_2O}^{eq}}{p_{H_2}^{eq}\,(p_{O_2}^{eq})^{1/2}} = \exp\left(-\frac{\Delta_r G_{\mathrm{WFR}}^\circ(T)}{RT}\right). \quad [28]$$

The defect equilibrium conditions according to Eqs. 23, 24 and 25 can only be fulfilled if the gas phase is equilibrated with respect to reaction 5. Otherwise, defect reactions HIR (Eq. 20), OIR (Eq. 21) and WIR (Eq. 22) consume surplus gas species and produce missing ones. Here, the following mass-action law rate equations are used for quantification.[25] These rate expressions are a simplification on the basis of the global reactions HIR, OIR and WIR and do not fully consider the complexity of the gas incorporation process: Incorporation may consist of several elementary kinetic reaction steps and the rate determining step may differ between materials.[65] Nevertheless, the equations used here are thermodynamically consistent and thus represent a reasonable choice in the context of electrochemical cell simulation:

$$\dot{q}_{\mathrm{HIR}} = k_{f,H_2}[O_O^\bullet][H_2]^{1/2} - k_{b,H_2}[OH_O^\bullet], \quad [29]$$

$$\dot{q}_{\mathrm{OIR}} = k_{f,O_2}[V_O^{\bullet\bullet}][O_O^x][O_2]^{1/2} - k_{b,O_2}[O_O^\bullet]^2, \quad [30]$$

$$\dot{q}_{\mathrm{WIR}} = k_{f,H_2O}[V_O^{\bullet\bullet}][O_O^x][H_2O] - k_{b,H_2O}[OH_O^\bullet]^2. \quad [31]$$

The reaction rates $\dot{q}$ relate to the defect production rates $\dot{s}_k$ as

$$\dot{s}_{V_O^{\bullet\bullet}} = -\dot{q}_{\mathrm{OIR}} - \dot{q}_{\mathrm{WIR}}, \quad [32]$$

$$\dot{s}_{OH_O^\bullet} = 2\dot{q}_{\mathrm{WIR}} + \dot{q}_{\mathrm{HIR}}, \quad [33]$$

$$\dot{s}_{O_O^\bullet} = 2\dot{q}_{\mathrm{OIR}} - \dot{q}_{\mathrm{HIR}} = -\dot{s}_{OH_O^\bullet} - 2\dot{s}_{V_O^{\bullet\bullet}}, \quad [34]$$

$$\dot{s}_{O_O^x} = -\dot{q}_{\mathrm{OIR}} - \dot{q}_{\mathrm{WIR}} = -\dot{s}_{O_O^\bullet} - \dot{s}_{V_O^{\bullet\bullet}} - \dot{s}_{OH_O^\bullet}. \quad [35]$$

The gas-phase production rates associated with defect-incorporation reactions can be expressed as

$$\dot{s}_{H_2} = -\dot{q}_{\mathrm{HIR}}/2, \quad [36]$$

$$\dot{s}_{O_2} = -\dot{q}_{\mathrm{OIR}}/2, \quad [37]$$

$$\dot{s}_{H_2O} = -\dot{q}_{\mathrm{WIR}}. \quad [38]$$

The oxygen-lattice site constraint for the ABO_3 perovskites remains fulfilled during reactions,

$$[V_O^{\bullet\bullet}]_L + [OH_O^\bullet]_L + [O_O^\bullet]_L + [O_O^x]_L = 3. \quad [39]$$

Charge neutrality within the ceramic electrolyte provides an additional constraint, whereby the negative charge comes from the B-site

doping as

$$2[V_O^{\bullet\bullet}]_L + [OH_O^{\bullet}]_L + [O_O^{\bullet}]_L - [X_B']_L = 0. \quad [40]$$

In case of $BaCe_{0.7}Zr_{0.1}Y_{0.1}Yb_{0.1}O_{3-\delta}$, the in Kröger–Vink notation negatively charged dopants in the ABO_3 perovskite crystal base structure are yttrium and ytterbium, represented in sum as X_B'. The overall dopant concentration on the lattice scale (mol/mol) is represented by $[X_B']_L$. It is related to the molar concentration as

$$[X_B]_L = [X_B]\, V_m, \quad [41]$$

where $V_m = 5.1323 \times 10^{-5}$ m^3/mol is the molar volume of BCZYYb.[16]

In materials such as BCZYYb, with multiple mobile charge carriers, charge neutrality can be realized with various combinations of mobile charged defect concentrations, based on the contacting gas phase composition. In contrast, in SCDC materials such as YSZ, the chemical potential of the positively charged defect is gas-phase independent and the concentration given by the doping instead. Assuming $V_O^{\bullet\bullet}$ as only mobile species in an SCDC (Eq. 40) thus simplifies to

$$2[V_O^{\bullet\bullet}]_L - [X_B']_L = 0. \quad [42]$$

Next to incorporation reactions HIR (Eq. 20), OIR (Eq. 21), and WIR (Eq. 22), mobile defects $OH_O^{\bullet}$, $V_O^{\bullet\bullet}$ and $O_O^{\bullet}$ in BCZYYb are produced and consumed through CT reactions, as shown exemplary in Fig. 3 for $OH_O^{\bullet}$ from water. In contrast to incorporation, CT reactions release or consume electrons in exchange with the electron conducting phase. Based on the available mobile defects, the considered CT reactions are H_2-vacancy-charge-transfer (HVCT, Eq. 1) and H_2-proton-charge-transfer (HHCT, Eq. 8) in the negatrode and O_2-vacancy-charge-transfer (OVCT, Eq. 2) alongside O_2-proton-charge-transfer (OHCT, Eq. 9) in the positrode. Additionally, an electrochemical reaction producing leakage current charge carriers is represented as polaron-charge-transfer (PCT),[25]

$$O_O^{x}(\mathrm{el}) \rightleftharpoons O_O^{\bullet}(\mathrm{el}) + e'(\mathrm{ed}). \quad [43]$$

This realtionship results from combining the hole-localization reaction (Eq. 19) and the electron-hole recombination reaction[55,66,67] as

$$\mathrm{null} \rightleftharpoons h^{\bullet} + e'. \quad [44]$$

Having identified the relevant CT reactions, as well as the dependencies of species activities on thermodynamic parameters, equilibrium potentials can be investigated in the case of thermodynamically equilibrated and non-equilibrated reactant supply.

Multiple CT reactions - species equilibrated.—In the following, equilibrium potentials in systems with multiple mobile charge carriers are calculated, using PCCs as illustrative example. It is assumed in this Section that all species in the same half cell are thermodynamically equilibrated. It is shown that even in presence of multiple charge carriers, equilibrium potentials of all CT reactions in the same half cell consequently are identical, leading to an unambiguous reversible cell potential. Further, the potential contributions which are missing in each of the two gas-phase based Nernst potentials $E^{\mathrm{V\,CR}}_{\mathrm{Nernst(gas)}}$ (Eq. 4) and $E^{\mathrm{HCR}}_{\mathrm{Nernst(gas)}}$ (Eq. 6) for a correct calculation of the actual reversible cell potential are identified.

Gases supplied to ceramic-based fuel cell are frequently thermodynamically equilibrated, due to the elevated operation temperatures and therefore increased gas and surface kinetics. Considering two separate half cells as shown in Fig. 1 with humid hydrogen in the negatrode and humid air in the positrode, the equilibrium partial pressures of O_2 in the H_2 fuel, as well as H_2 in the air can each be calculated from the water formation equilibrium constant according to Eq. 28. Defect incorporation reactions are equilibrated according to Eqs. 23, 24, and 25. Reactions HHCT (Eq. 8), HVCT (Eq. 1) and PCT (Eq. 43) represent the CT reactions occurring in the negatrode, reactions OHCT (Eq. 9), OVCT (Eq. 2) and again PCT (Eq. 43) are present in the positrode. The respective CT equilibrium potentials according to Eq. 15 are as follows in the negatrode:

$$E_{\mathrm{nt}}^{\mathrm{eq,HHCT}} = \frac{2\mu^{\circ}_{OH_O^{\bullet}} + 2\mu^{\circ}_{e'} - \mu^{\circ}_{H_2} - 2\mu^{\circ}_{O_O^{x}}}{2F} + \frac{RT}{2F}\ln\left(\frac{([OH_O^{\bullet}]_{\mathrm{nt}})^2\, p^{\circ}}{([O_O^{x}]_{\mathrm{nt}})^2\, p_{H_2,\mathrm{nt}}}\right), \quad [45]$$

$$E_{\mathrm{nt}}^{\mathrm{eq,HV\,CT}} = \frac{\mu^{\circ}_{H_2O} + \mu^{\circ}_{V_O^{\bullet\bullet}} + 2\mu^{\circ}_{e'} - \mu^{\circ}_{H_2} - \mu^{\circ}_{O_O^{x}}}{2F} + \frac{RT}{2F}\ln\left(\frac{[V_O^{\bullet\bullet}]_{\mathrm{nt}}\, p_{H_2O,\mathrm{nt}}}{[O_O^{x}]_{\mathrm{nt}}\, p_{H_2,\mathrm{nt}}}\right), \quad [46]$$

$$E_{\mathrm{nt}}^{\mathrm{eq,PCT}} = \frac{\mu^{\circ}_{O_O^{\bullet}} + \mu^{\circ}_{e'} - \mu^{\circ}_{O_O^{x}}}{F} + \frac{RT}{F}\ln\left(\frac{[O_O^{\bullet}]_{\mathrm{nt}}}{[O_O^{x}]_{\mathrm{nt}}}\right). \quad [47]$$

Similarly, at the positrode,

$$E_{\mathrm{pt}}^{\mathrm{eq,OHCT}} = \frac{2\mu^{\circ}_{OH_O^{\bullet}} + 2\mu^{\circ}_{e'} + \frac{1}{2}\mu^{\circ}_{O_2} - 2\mu^{\circ}_{O_O^{x}} - \mu^{\circ}_{H_2O}}{2F} + \frac{RT}{2F}\ln\left(\frac{(p_{O_2,\mathrm{pt}})^{1/2}\,([OH_O^{\bullet}]_{\mathrm{pt}})^2\,(p^{\circ})^{1/2}}{p_{H_2O,\mathrm{pt}}\,([O_O^{x}]_{\mathrm{pt}})^2}\right), \quad [48]$$

$$E_{\mathrm{pt}}^{\mathrm{eq,OV\,CT}} = \frac{\frac{1}{2}\mu^{\circ}_{O_2} + \mu^{\circ}_{V_O^{\bullet\bullet}} + 2\mu^{\circ}_{e'} - \mu^{\circ}_{O_O^{x}}}{2F} + \frac{RT}{2F}\ln\left(\frac{[V_O^{\bullet\bullet}]_{\mathrm{pt}}\,(p_{O_2,\mathrm{pt}})^{1/2}}{[O_O^{x}]_{\mathrm{pt}}\,(p^{\circ})^{1/2}}\right), \quad [49]$$

$$E_{\mathrm{pt}}^{\mathrm{eq,PCT}} = \frac{\mu^{\circ}_{O_O^{\bullet}} + \mu^{\circ}_{e'} - \mu^{\circ}_{O_O^{x}}}{F} + \frac{RT}{F}\ln\left(\frac{[O_O^{\bullet}]_{\mathrm{pt}}}{[O_O^{x}]_{\mathrm{pt}}}\right). \quad [50]$$

Since each half cell is in thermodynamic equilibrium, the gas phase partial pressures and defect concentrations represent equilibrium values. Consequently, each CT reaction can be expressed through linear combinations of other equilibrated (CT) reactions. This is shown in exemplary by combining the electrochemically equilibrated H_2 oxidation reaction HHCT (Eq. 8) with the equilibrated H_2 incorporation reaction HIR (Eq. 20), resulting in the electrochemically equilibrated CT reaction PCT (43).

Using Eqs. 13 and 16, the electrochemical Gibbs energy equation for the equilibrated CT reaction HHCT (Eq. 8) may be represented as

$$\Delta_r\widetilde{G}_{\mathrm{HHCT}} = 2\widetilde{\mu}_{OH_O^{\bullet}} + 2\widetilde{\mu}_{e'} - \mu_{H_2} - 2\mu_{O_O^{x}} = \Delta_r G_{\mathrm{HHCT}} - 2FE_{\mathrm{nt}}^{\mathrm{eq,HHCT}} = 0. \quad [51]$$

Further, since the HIR (Eq. 20) is equilibrated, its (electro)chemical Gibbs energy is also zero:

$$\Delta_r\widetilde{G}_{\mathrm{HIR}} = -\frac{1}{2}\mu_{H_2} - \widetilde{\mu}_{O_O^{\bullet}} + \widetilde{\mu}_{OH_O^{\bullet}} = \Delta_r G_{\mathrm{HIR}} = 0. \quad [52]$$

Linearly combining Eqs. 51 and 52, the definition of the electrochemical Gibbs energy for the PCT reaction is recovered as

$$\frac{1}{2}\Delta_r\widetilde{G}_{HHCT} - \Delta_r G_{HIR} = \widetilde{\mu}_{O_O^\bullet} + \widetilde{\mu}_{e'} - \mu_{O_O^x} = \Delta_r\widetilde{G}_{PCT} = 0. \quad [53]$$

Perhaps as may be anticipated, the O_O^x oxidation reaction PCT (Eq. 43) is also equilibrated, since $\Delta_r\widetilde{G}_{PCT} = 0$. It can be shown that this implies that both charge transfer reactions HHCT (Eq. 8) and PCT (Eq. 43) share the same CT equilibrium potential: Reformulating Eq. 53, using Eq. 51 leads to

$$\Delta_r\widetilde{G}_{PCT} = \frac{1}{2}(\Delta_r G_{HHCT} - 2FE_{nt}^{eq,HHCT}) - \Delta_r G_{HIR} = 0. \quad [54]$$

Expressing $\Delta_r G_{HHCT}$ and $\Delta_r G_{HIR}$ as chemical potentials according to Eq. 13 and combining them results in $\Delta_r G_{PCT}$ as

$$\frac{1}{2}\Delta_r G_{HHCT} - \Delta_r G_{HIR} = \Delta_r G_{PCT}. \quad [55]$$

Consequently, Eq. 54 can be rewritten as

$$\Delta_r\widetilde{G}_{PCT} = \Delta_r G_{PCT} - FE_{nt}^{eq,HHCT} = 0. \quad [56]$$

A comparison between the obtained equation and the definition of the CT equilibrium potential for PCT reaction (Eq. 43), expressed as

$$\Delta_r\widetilde{G}_{PCT} = \Delta_r G_{PCT} - FE_{nt}^{eq,PCT} = 0, \quad [57]$$

reveals that

$$E_{nt}^{eq,PCT} = E_{nt}^{eq,HHCT}. \quad [58]$$

Thus, the CT equilibrium potential $E_{nt}^{eq,HHCT}$ from the CT reaction HHCT (Eq. 8) producing $OH_O^\bullet$ from H_2 also equilibrates the second CT reaction PCT (Eq. 43) producing $O_O^\bullet$ from O_O^x. It is generally true that two electrochemically equilibrated CT reactions that can be transformed into one another through linear combinations with other equilibrated reactions will share the same equilibrium potential. If all species in the half cell are thermodynamically equilibrated this implies that there is a single half cell equilibrium potential E^{eq} for all CT reactions in the same half cell. For example, the CT equilibrium potentials in the PCC negatrode may be expressed as

$$E_{nt}^{eq,HHCT} = E_{nt}^{eq,HV\,CT} = E_{nt}^{eq,PCT} = E_{nt}^{eq}. \quad [59]$$

Similarly, at the positrode

$$E_{pt}^{eq,OHCT} = E_{pt}^{eq,OV\,CT} = E_{pt}^{eq,PCT} = E_{pt}^{eq}. \quad [60]$$

The resulting potential difference across two half cells, according to Eq. 18 is the unambiguous, reversible cell potential[68] as

$$E_{pt}^{eq} - E_{nt}^{eq} = \Delta E^{eq} = E_{rev}. \quad [61]$$

For example, E_{rev} can be obtained from CT reaction HHCT (Eq. 8) in the negatrode and OHCT (Eq 9) in the positrode, which combined, result in the HCR (Eq. 7) as

$$\begin{aligned} E_{rev} = \Delta E^{eq,HCR} &= E_{pt}^{eq,OHCT} - E_{nt}^{eq,HHCT} \\ &= -\frac{\Delta_r G^\circ_{WFR}(T)}{2F} + \underbrace{\frac{RT}{2F}\ln\left(\frac{(p^{eq}_{O_2,pt})^{1/2}\,p^{eq}_{H_2,nt}}{p^{eq}_{H_2O,pt}\,(p^\circ)^{1/2}}\right)}_{E^{HCR}_{Nernst(gas)}} \\ &\quad + \underbrace{\frac{RT}{2F}\ln\left(\frac{([OH_O^\bullet]^{eq}_{pt})^2\,([O_O^x]^{eq}_{nt})^2}{([OH_O^\bullet]^{eq}_{nt})^2\,([O_O^x]^{eq}_{pt})^2}\right)}_{E^{HCR}_{Nernst(def.)}}. \end{aligned} \quad [62]$$

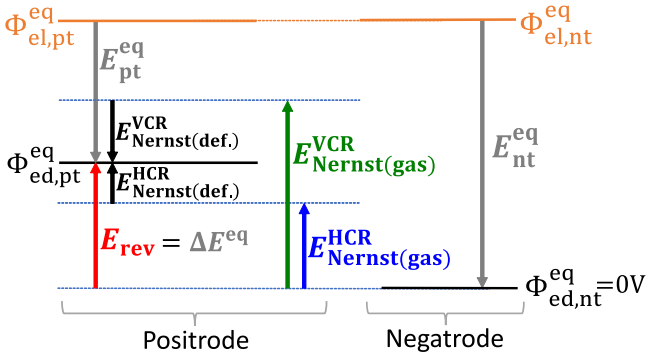

Figure 4. Electrostatic potentials in case of thermodynamically equilibrated gas and defect species in separated half cells. The reversible cell potential E_{rev} is clearly defined.

$E^{HCR}_{Nernst(gas)}$ is the gas-phase-based Nernst equation (Eq. 6) and $E^{HCR}_{Nernst(def.)}$ is a defect based Nernst potential contribution.

Alternatively, from half-cell reactions HVCT (Eq. 1) and OVCT (Eq. 2) (combining to VCR (Eq. 3)):

$$\begin{aligned} E_{rev} = \Delta E^{eq,V\,CR} &= E_{pt}^{eq,OV\,CT} - E_{nt}^{eq,HV\,CT} \\ &= -\frac{\Delta_r G^\circ_{WFR}(T)}{2F} + \underbrace{\frac{RT}{2F}\ln\left(\frac{(p^{eq}_{O_2,pt})^{1/2}\,p^{eq}_{H_2,nt}}{p^{eq}_{H_2O,nt}\,(p^\circ)^{1/2}}\right)}_{E^{VCR}_{Nernst(gas)}} \\ &\quad + \underbrace{\frac{RT}{2F}\ln\left(\frac{[V_O^{\bullet\bullet}]^{eq}_{pt}\,[O_O^x]^{eq}_{nt}}{[V_O^{\bullet\bullet}]^{eq}_{nt}\,[O_O^x]^{eq}_{pt}}\right)}_{E^{VCR}_{Nernst(def.)}}. \end{aligned} \quad [63]$$

Combining $E_{pt}^{eq,PCT}$ and $E_{nt}^{eq,PCT}$ yields yet another (and possibly the simplest) expression for the reversible cell potential E_{rev}:[26,30]

$$\begin{aligned} E_{rev} = \Delta E^{eq,PCT} &= E_{pt}^{eq,PCT} - E_{nt}^{eq,PCT} \\ &= \frac{RT}{F}\ln\left(\frac{[O_O^\bullet]^{eq}_{pt}\,[O_O^x]^{eq}_{nt}}{[O_O^\bullet]^{eq}_{nt}\,[O_O^x]^{eq}_{pt}}\right). \end{aligned} \quad [64]$$

In summary, in a cell with multiple mobile charge carriers, the equilibrium half-cell potentials obtained for all the charge transfer reactions are equivalent in case all species are thermodynamically equilibrated. Further, the reversible cell potential is shown to be unambiguous irrespective of the specific charge transfer reactions it is derived from. Notably, the reversible cell potential E_{rev} derived according to Eq. 62 or Eq. 63 contains the gas-phase based Nernst potentials $E^{HCR}_{Nernst(gas)}$ (Eq. 6) and $E^{V\,CR}_{Nernst(gas)}$ (Eq. 4), as illustrated qualitatively in Fig. 4 as blue and green arrows respectively. This resolves the ambiguity of the purely gas-phase based Nernst equations in defining the reversible cell potential, since E_{rev} includes the unifying terms $E^{HCR}_{Nernst(def.)}$ and $E^{V\,CR}_{Nernst(def.)}$ (black arrows in Fig. 4). These term quantify the energy contribution of defect concentration differences between the electrodes which can occur in cells with multiple mobile charge carriers. E_{rev} (red arrow) can thus be understood as the complete Nernst equation for the cell.

In electrodes based on SCDCs like YSZ, the charged local defect concentration $V_O^{\bullet\bullet}$ and O_O^x is uniform and defined purely by the electrolyte doping according to Eq. 42. Consequently, in case of equal electrolytes in both half cells $E^{V\,CR}_{Nernst(def.)}$ becomes 0 and E_{rev} can be calculated directly from the gas phase composition.[69] In contrast, in cells with multiple mobile charge carriers, equilibrium defect concentrations can be dependent on the gas-phase

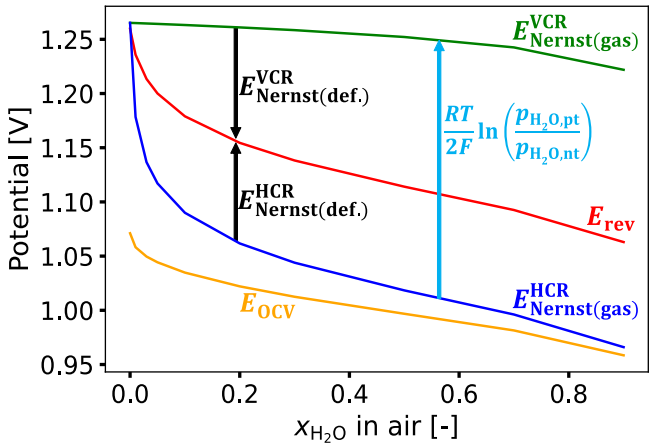

Figure 5. Equilibrium potentials given at 600 °C for BCZYYb-based half cells with increasing mole fraction of water x_{H_2O} in the positrode. O_2 content in air is reduced with increasing H_2O content. Negatrode contains 0.1 mol% H_2O in H_2 fuel. Trace H_2 and O_2 are calculated according to WFR equilibrium for positrode and negatrode half cell respectively. Thermodynamic parameters are from Table I. E_{OCV} is simulated using parameters from Tables II, III and IV.

compositions, as is the case for BCZYYb according to incorporation reactions HIR (Eq. 20), OIR (Eq. 21) and WIR (Eq. 22). This dependency of defect based Nernst potential contributions ($E^{HCR}_{Nernst(def.)}$ and $E^{V\,CR}_{Nernst(def.)}$) of the gas phase composition is illustrated in Fig. 5. The Figure shows the various potentials of a BCZYYb-based cell where the negatrode contains slightly humidified hydrogen (0.1 mol% H_2O in H_2 fuel), while in the positrode the humidity is varied. With increasing humidity difference, the magnitude of both defect based potential contributions $E^{V\,CR}_{Nernst(def.)}$ and $E^{HCR}_{Nernst(def.)}$ (black arrows) increases. Additionally, the reversible cell potential E_{rev} (red line) is also distinct from the gas-phase based Nernst-potentials (blue and green lines). For reference, Fig. 5 also includes calculated values for the open-circuit voltage E_{OCV} (orange line), which represents the measurable voltage of a fully assembled cell as shown in Fig. 3 at the absence of electric current through the outer circuit. As explained more closely in Section "Open Circuit Voltage" below, E_{OCV} is lower than E_{rev} due to transference numbers of various defects being non-zero in a cell at open circuit conditions. OCV calculations are based on cell- and reaction parameters given in Tables II, III and IV.

By varying the mole fraction of water x_{H_2O}, Fig. 5 illustrates how defect based Nernst potential contributions $E_{Nernst(def.)}$ influence the reversible cell potential E_{rev} in a cell capable of conducting multiple mobile charge carriers. Figure 5 also shows that the consideration of $E_{Nernst(def.)}$ in the calculation of the reversible cell potential does not violate thermodynamic principles as the energy contribution from the defects indirectly traces back to chemical potential differences of gas species, in this case a partial pressure difference in water vapor. Differently phrased, some of the Gibbs energy difference between gases supplied to the electrochemical system may not be available as electrical energy output (i.e. reversible work). Instead, it is required to uphold a concentration difference of otherwise mobile charged species across the electrolyte. Thus, in a system with multiple charge carriers, the reversible potential E_{rev} and gas-phase based Nernst potentials $E_{Nernst(gas)}$ can differ.

Interfacial cell models assume that all species participating in any charge transfer reaction are in thermodynamic equilibrium at every location within the electrode. These models can therefore use the value of E_{rev} to simulate a (polarized) cell without violating thermodynamic consistency. Examples for correct application can be found in[16] or.[29]

Multiple CT reactions - species not equilibrated.—This Section shows that the presence of thermodynamically non-equilibrated species in the electrode leads to diverging CT equilibrium potentials $E^{eq,r}$ for individual CT reactions. Consequently, the calculation of a single reversible cell potential, at which all CT reactions are thermodynamically equilibrated, is not possible. Instead, mixed-potential theory can be used to calculate a steady-state mixed cell potential, at which ceramic defect concentrations and potentials are time-invariant, while reactant gas species are constantly consumed/produced, according to their deviation from equilibrium concentration. (Nevertheless, the gas composition is considered fixed, representing a flushed electrode). The concept of zero charge- or species flux between the half cells continues to be applied in this discussion, which allows for the calculated mixed cell potential to serve as theoretical reference value for measurements in assembled cells which include a dense electrolyte membrane between the electrodes.

The disparity of CT equilibrium potentials in case of non-equilibrated species in the half cell can be illustrated conceptionally on the example of a negatrode gas supply consisting of H_2, NH_3, N_2 and H_2O in which the species H_2, NH_3 and N_2 are not thermodynamically equilibrated according to the ammonia formation reaction (AFR) reaction:

$$0.5\,N_2(g) + 1.5\,H_2(g) \rightleftharpoons NH_3(g). \qquad [65]$$

Therefore, its Gibbs energy $\Delta_r G_{AFR}(T)$ (calculated according to Eq. 13) is non-zero. Other than in the gas phase or thermocatalytically, NH_3 may react in an ammonia-proton-charge-transfer (AHCT),[33,71,72] similar to the H_2-proton-charge-transfer reaction (HHCT, Eq. 8):

$$NH_3(g) + 3\,O^x_O(el) \rightleftharpoons 3\,OH^\bullet_O(el) + 0.5\,N_2(g) + 3\,e'(ed). \qquad [66]$$

According to Eq. 15), the CT equilibrium potential for NH_3 oxidation may be evaluated as

$$E^{eq,AHCT}_{nt} = \frac{3\mu^\circ_{OH^\bullet_O} + \frac{1}{2}\mu^\circ_{N_2} + 3\mu^\circ_{e'} - \mu^\circ_{NH_3} - 3\mu^\circ_{O^x_O}}{3F} + \frac{RT}{3F}\ln\left(\frac{([OH^\bullet_O]_{nt})^3\,(p_{N_2,nt})^{1/2}\,(p^\circ)^{1/2}}{([O^x_O]_{nt})^3\,p_{NH_3,nt}}\right). \qquad [67]$$

The difference between both equilibrium potentials $E^{eq,AHCT}_{nt}$ and $E^{eq,HHCT}_{nt}$ in the same electrode is non-zero since $\Delta_r G_{AFR}(T) \neq 0$,

$$E^{eq,AHCT}_{nt} - E^{eq,HHCT}_{nt} = \frac{\frac{1}{2}\mu^\circ_{N_2} + \frac{3}{2}\mu^\circ_{H_2} - \mu^\circ_{NH_3}}{3F} + \frac{RT}{3F}\ln\left(\frac{(p_{N_2,nt})^{1/2}\,(p_{H_2,nt})^{3/2}}{p_{NH_3,nt}\;p^\circ}\right) = -\frac{\Delta_r G_{AFR}(T)}{3F} \neq 0. \qquad [68]$$

Analogously, $E^{eq,HHCT}$, $E^{eq,HV\ CT}$ and $E^{eq,PCT}$ diverge if H_2, O_2 and H_2O are not equilibrated according to Eq. 28, since the Gibbs energies of incorporation reactions HIR (Eq. 20), OIR (Eq. 21) and WIR (Eq. 22) cannot be zero simultaneously.

Consequently, no common thermodynamic half cell equilibrium potential E^{eq}_{nt} or reversible cell potential E_{rev} exists, leading to a non-zero overpotential η^r for at least one of the CT reactions r:[25]

$$\eta^r = E - E^{eq,r} = \Phi_{ed} - \Phi_{el} - (\Phi^{eq,r}_{ed} - \Phi^{eq,r}_{el}). \qquad [69]$$

This overpotential leads to a source of electric current i^r, frequently quantified through the Butler–Volmer equation as $i^r = f(i^{0,r}, \eta^r)$, which can be derived from mass-action kinetics.[11] $i^{0,r}$

is the exchange current density. (An example of a Butler–Volmer formulation for half-cell reaction HHCT is represented by Eq. 90).

$E^{\mathrm{eq},r}$ in η^r contains unknown standard state chemical potentials $\mu^\circ_{\mathrm{OH}^\bullet_\mathrm{O}}$, $\mu^\circ_{\mathrm{V}^{\bullet\bullet}_\mathrm{O}}$, $\mu^\circ_{\mathrm{O}^\bullet_\mathrm{O}}$, $\mu^\circ_{\mathrm{O}^\mathrm{x}_\mathrm{O}}$ and $\mu^\circ_{\mathrm{e}'}$ which can be removed by applying a reference shift γ [73] on the electrolyte material (equilibrium) potentials Φ_el and $\Phi^{\mathrm{eq},r}_\mathrm{el}$, without changing the overpotential η^r from Eq. 69. That is,

$$\begin{aligned}\eta^r &= E - E^{\mathrm{eq},r}\\ &= \Phi_\mathrm{ed} - [\Phi_\mathrm{el} - \gamma] - (\Phi^{\mathrm{eq},r}_\mathrm{ed} - [\Phi^{\mathrm{eq},r}_\mathrm{el} - \gamma])\\ &= \Phi_\mathrm{ed} - \hat{\Phi}_\mathrm{el} - (\Phi^{\mathrm{eq},r}_\mathrm{ed} - \hat{\Phi}^{\mathrm{eq},r}_\mathrm{el}) = \hat{E} - \hat{E}^{\mathrm{eq},r},\end{aligned} \tag{70}$$

with

$$\hat{E}^{\mathrm{eq},r} = E^{\mathrm{eq},r} + \gamma, \tag{71}$$

and

$$\hat{\Phi}^{\mathrm{eq},r}_\mathrm{el} = \Phi^{\mathrm{eq},r}_\mathrm{el} - \gamma. \tag{72}$$

and equally for their non-equilibrated counterparts E and Φ_el.

It is essential that γ be chosen such that it contains and removes all unknowns from all CT equilibrium potentials $E^{\mathrm{eq},r}$ in both positrode and negatrode. For instance, with the specific reference shift,

$$\gamma = \frac{\mu^\circ_{\mathrm{O}^\mathrm{x}_\mathrm{O}} - \mu^\circ_{\mathrm{O}^\bullet_\mathrm{O}} - \mu^\circ_{\mathrm{e}'}}{F}, \tag{73}$$

the previously derived CT equilibrium potentials (Eq. 45) to (Eq. 50) are shifted, returning for the negatrode

$$\hat{E}^{\mathrm{eq,HHCT}}_\mathrm{nt} = \frac{2\,\Delta_\mathrm{r}G^\circ_\mathrm{HIR}(T)}{2F} + \frac{RT}{2F}\ln\left(\frac{([\mathrm{OH}^\bullet_\mathrm{O}]_\mathrm{nt})^2\,p^\circ}{([\mathrm{O}^\mathrm{x}_\mathrm{O}]_\mathrm{nt})^2\,p_{\mathrm{H_2,nt}}}\right), \tag{74}$$

$$\hat{E}^{\mathrm{eq,HV\,CT}}_\mathrm{nt} = \frac{2\,\Delta_\mathrm{r}G^\circ_\mathrm{HIR}(T) - \Delta_\mathrm{r}G^\circ_\mathrm{WIR}(T)}{2F} + \frac{RT}{2F}\ln\left(\frac{[\mathrm{V}^{\bullet\bullet}_\mathrm{O}]_\mathrm{nt}\,p_{\mathrm{H_2O,nt}}}{[\mathrm{O}^\mathrm{x}_\mathrm{O}]_\mathrm{nt}\,p_{\mathrm{H_2,nt}}}\right), \tag{75}$$

$$\hat{E}^{\mathrm{eq,PCT}}_\mathrm{nt} = 0 + \frac{RT}{F}\ln\left(\frac{[\mathrm{O}^\bullet_\mathrm{O}]_\mathrm{nt}}{[\mathrm{O}^\mathrm{x}_\mathrm{O}]_\mathrm{nt}}\right). \tag{76}$$

Analogously, for the positrode,

$$\hat{E}^{\mathrm{eq,OHCT}}_\mathrm{pt} = \frac{2\,\Delta_\mathrm{r}G^\circ_\mathrm{HIR}(T) - \Delta_\mathrm{r}G^\circ_\mathrm{WFR}(T)}{2F} + \frac{RT}{2F}\ln\left(\frac{(p_{\mathrm{O_2,pt}})^{1/2}\,([\mathrm{OH}^\bullet_\mathrm{O}]_\mathrm{pt})^2\,(p^\circ)^{1/2}}{p_{\mathrm{H_2O,pt}}\,([\mathrm{O}^\mathrm{x}_\mathrm{O}]_\mathrm{pt})^2}\right), \tag{77}$$

$$\hat{E}^{\mathrm{eq,OV\,CT}}_\mathrm{pt} = \frac{-\Delta_\mathrm{r}G^\circ_\mathrm{OIR}(T)}{2F} + \frac{RT}{2F}\ln\left(\frac{[\mathrm{V}^{\bullet\bullet}_\mathrm{O}]_\mathrm{pt}\,(p_{\mathrm{O_2,pt}})^{1/2}}{[\mathrm{O}^\mathrm{x}_\mathrm{O}]_\mathrm{pt}\,(p^\circ)^{1/2}}\right), \tag{78}$$

$$\hat{E}^{\mathrm{eq,PCT}}_\mathrm{pt} = 0 + \frac{RT}{F}\ln\left(\frac{[\mathrm{O}^\bullet_\mathrm{O}]_\mathrm{pt}}{[\mathrm{O}^\mathrm{x}_\mathrm{O}]_\mathrm{pt}}\right). \tag{79}$$

With

$$\Delta_\mathrm{r}G^\circ_\mathrm{HIR}(T) = \mu^\circ_{\mathrm{OH}^\bullet_\mathrm{O}} - 0.5\mu^\circ_{\mathrm{H_2}} - \mu^\circ_{\mathrm{O}^\bullet_\mathrm{O}} = -RT\,\ln(K_{p,\mathrm{HIR}}) \tag{80}$$

and $K_{p,\mathrm{HIR}}$ from Eq. 23), calculated from known material parameters listed in Table I. Similarly for $\Delta_\mathrm{r}G^\circ_\mathrm{OIR}(T)$ and $\Delta_\mathrm{r}G^\circ_\mathrm{WIR}(T)$:

$$\Delta_\mathrm{r}G^\circ_\mathrm{OIR}(T) = -RT\,\ln(K_{p,\mathrm{OIR}}), \tag{81}$$

$$\Delta_\mathrm{r}G^\circ_\mathrm{WIR}(T) = -RT\,\ln(K_{p,\mathrm{WIR}}). \tag{82}$$

Shifting the CT equilibrium potential of the ammonia oxidation reaction AHCT (66) by γ as given in (73) leads to:

$$\hat{E}^{\mathrm{eq,AHCT}}_\mathrm{nt} = \frac{3\Delta_\mathrm{r}G^\circ_\mathrm{HIR}(T) - \Delta_\mathrm{r}G^\circ_{\mathrm{g},\mathrm{NH_3}}(T)}{3F} + \frac{RT}{3F}\ln\left(\frac{([\mathrm{OH}^\bullet_\mathrm{O}]_\mathrm{nt})^3\,(p_{\mathrm{N_2,nt}})^{1/2}\,(p^\circ)^{1/2}}{([\mathrm{O}^\mathrm{x}_\mathrm{O}]_\mathrm{nt})^3\,p_{\mathrm{NH_3,nt}}}\right), \tag{83}$$

with the standard Gibbs energy $\Delta_\mathrm{r}G^\circ_{\mathrm{g},\mathrm{NH_3}}(T)$ corresponding to the gas phase reaction (65). Consequently, all $\hat{E}^{\mathrm{eq},r}$ can be calculated.

According to mixed-potential theory, isolated half cells exposed to a non-equilibrated gas phase adopt a potential difference E, such that the sum of the currents produced by individual CT reactions $\mathbf{R}_\mathrm{CT}$ in the half cell sum to zero[74–76] as

$$i = \sum_{r\,\in\,\mathbf{R}_\mathrm{CT}} i^r = 0. \tag{84}$$

However, CT reactions do not only change the electron balance, but also produce gas species and ceramic defects. Since the gas phase is considered fixed (electrodes are flushed), gas phase source terms can be neglected and a mass balance needs to be fulfilled only for defects $k \in \{\mathrm{V}^{\bullet\bullet}_\mathrm{O}, \mathrm{OH}^\bullet_\mathrm{O}, \mathrm{O}^\bullet_\mathrm{O}\}$, in order to avoid accumulation or depletion in the composite electrode. In PCCs, next to CT reactions, defect-incorporation rate equations, (Eqs. 29, 30, and Eq. 31) are also non-zero in case of a non-equilibrated gas phase, thus producing electrolyte species according to Eqs. (32), (33), (34) and (35). Therefore, the resulting mass balances for the charged defects k need to include both, incorporation rates $\dot{s}_k$ and contributions from CT reactions r,

$$\dot{s}_k + \frac{i^r}{z_k F} = 0. \tag{85}$$

Combining Eq. 85 for two of the three defects, Eq. 84, as well as the site constraint (Eq. 39) and the electroneutrality condition (Eq. 40) results in an algebraic equation system with five independent equations for five unknowns: $\hat{E}^{\mathrm{mix}}_\mathrm{nt}$, $[\mathrm{OH}^\bullet_\mathrm{O}]_\mathrm{nt}$, $[\mathrm{O}^\bullet_\mathrm{O}]_\mathrm{nt}$, $[\mathrm{V}^{\bullet\bullet}_\mathrm{O}]_\mathrm{nt}$ and $[\mathrm{O}^\mathrm{x}_\mathrm{O}]_\mathrm{nt}$. $\hat{E}^{\mathrm{mix}}_\mathrm{nt}$ is the half cell mixed potential, which ensures all mass and charge balances in the negatrode are closed. By subtracting $\hat{E}^{\mathrm{mix}}_\mathrm{nt}$ from the positrode half cell equilibrium potential $E^{\mathrm{eq}}_\mathrm{pt}$, the mixed cell potential ΔE^{mix} can be calculated in analogy with Eq. 18) as

$$\Delta E^{\mathrm{mix}} = \hat{E}^{\mathrm{eq}}_\mathrm{pt} - \hat{E}^{\mathrm{mix}}_\mathrm{nt}. \tag{86}$$

Just as the reversible cell potential E_rev, the mixed cell potential ΔE^{mix} cannot be measured experimentally in cells with multiple mobile charge carriers as it is based on the concept of separated half cells without a connecting electrolyte membrane. Figure 6a qualitatively illustrates the negatrode mixed potential formation $\hat{E}^{\mathrm{mix}}_\mathrm{nt}$ (pink arrow) in the presence of non-equilibrated H_2, NH_3 and N_2 in the negatrode. Humid air with equilibrated H_2 content in the positrode allows for O_2-proton-charge-transfer (OHCT, Eq. 9), resulting in the mixed cell potential ΔE^{mix} (red arrow). The existence of only two CT reactions HHCT (Eq. 8) and AHCT (Eq. 66) in the negatrode is assumed for better visualization. Their respective CT equilibrium potentials $\hat{E}^{\mathrm{eq,HHCT}}_\mathrm{nt}$ and $\hat{E}^{\mathrm{eq,AHCT}}_\mathrm{nt}$ (gray arrows) are not equal, leading

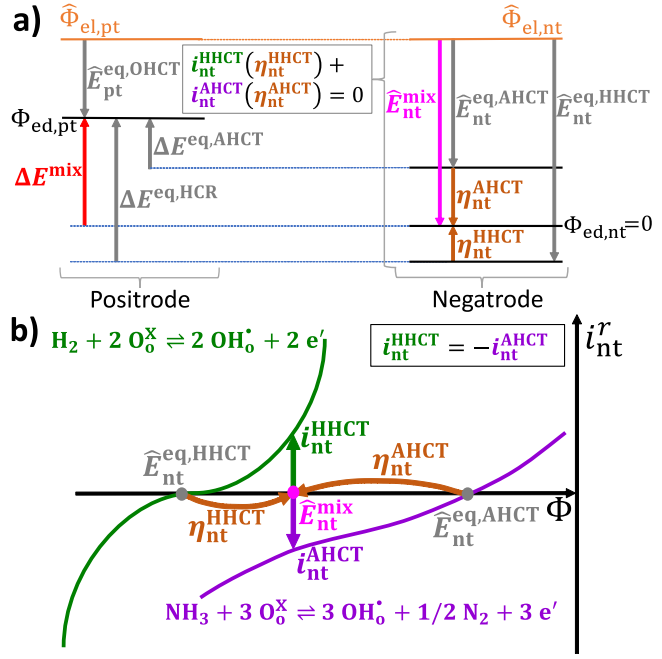

Figure 6. a) Electrostatic potentials in case of equilibrated humid air in the positrode and non-equilibrated H_2, NH_3 and N_2 in the negatrode. A mixed cell potential ΔE^{mix} is formed at steady-state which leads to the consumption of H_2 and production of NH_3. b) The value of $\hat{E}_{nt}^{mix}$ depends on the shape of the half-cell polarization curves of two competing CT reactions in the negatrode.

to overpotentials in the negatrode (brown arrows). Figure 6b qualitatively shows the influence of the charge transfer polarization kinetics on the exact position of the negatrode mixed potential $\hat{E}_{nt}^{mix}$ (pink dot).

Notably, the resulting mixed cell potential ΔE^{mix} (red arrow in Fig. 6) does not represent a thermodynamic equilibrium and is a steady-state value instead, i.e. defect concentrations and potentials are time-invariant. ΔE^{mix} differs from E_{rev}, which did not require kinetic considerations. The mixed cell potential ΔE^{mix} consequently originates from the field of non-equilibrium thermodynamics,[77] while a unique reversible cell potential E_{rev} which considers all CT reactions does not exist in presence of non-equilibrated species.

In the following, the formation of a mixed cell potential is investigated by hand of a realistic scenario for electrochemical NH_3 production in a cell forming H_2 and NH_3 in the negatrode in two competing CT reactions, as suggested conceptually by Okazaki et al.[33] In this work, a recirculated negatrode gas consisting of 3 mol% H_2 and 3 mol% H_2O (with equilibrated traces of O_2), and a NH_3 content of 10^{-6} mol%, with the remains being N_2 is assumed. Ammonia, hydrogen and nitrogen concentrations are not thermodynamically equilibrated, since the equilibrium ammonia content for the given gas phase at 600 °C would be more than two decades larger at $7.739 \cdot 10^{-4}$ mol%. The positrode may be fed a mixture of 97 mol% H_2O and 3 mol% O_2 as recirculated electrolysis product. The considered negatrode CT reactions are HHCT (Eq. 8), PCT (Eq. 43) and AHCT (Eq. 66), which combined with the positrode H_2O electrolysis reaction OHCT (9) produce a mixed cell potential ΔE^{mix}. Figure 7 shows ΔE^{mix} (red lines) as a function of exchange current density ratios $i^{0,AHCT}/i^{0,HHCT}$ for reactions AHCT (Eq. 8) and HHCT (Eq. 66) respectively with two different sets of defect-incorporation reaction rate constants: "slow" indicates defect incorporation forward rate constants corresponding to $BaZr_{0.9}Y_{0.1}O_{3-\delta}$ (BZY10)[60] (for lack of data for BCZYYb). Corresponding backward rate constants are calculated from the equilibrium constant for BCZYYb according to Eq. 26 for thermodynamic consistency. The index "fast" signifies incorporation rate constants were increased by a factor of 10^8, thus ensuring incorporation processes are non-limiting.

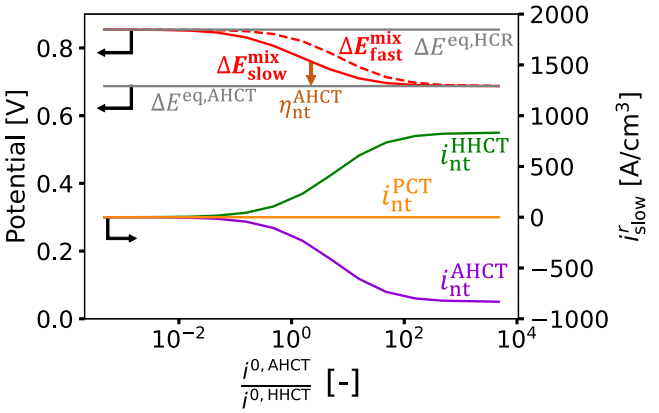

Figure 7. ΔE^{mix} for non-equilibrated NH_3 concentrations in the negatrode and two different sets of incorporation reaction rate constants, indexed "slow" and "fast". Charge transfer rates for negatrode reactions HHCT (Eq. 8), PCT (Eq. 43) and AHCT (Eq. 66) at 600 °C are given for the case of "slow" defect incorporation.

Depending on the exchange current density ratio, ΔE^{mix} is located between two thermodynamic extremes: $\Delta E^{eq,HCR}$ and $\Delta E^{eq,AHCT}$ (gray lines), leading to the formation of overpotentials η_{nt}^{AHCT} (brown arrow) and η_{nt}^{HHCT} (not shown). Negatrode CT rates i_{nt}^{r} given for the case of slow defect incorporation explain the dependency of ΔE^{mix} on kinetics: At comparatively high exchange current densities $i_{nt}^{0,AHCT}$ for the NH_3 oxidation reaction (right side of the graph), protons $OH_O^{\bullet}$ are produced from H_2 by CT reaction HHCT (8) (green line in Fig. 7) and consumed by the reversed CT reaction AHCT (66), producing NH_3 (violet line). This is thermodynamically reasonable, as the given ammonia partial pressure in the negatrode is below thermodynamic equilibrium. Since the exchange current density $i_{nt}^{0,AHCT}$ is high compared to i_{nt}^{HHCT}, the reaction is sensitive to overpotentials η_{nt}^{AHCT}, meaning the mixed cell potential will follow $\Delta E^{eq,AHCT}$ closely. In case of low $i_{nt}^{0,AHCT}$ on the other hand (left side of the graph), the mixed cell potential ΔE^{mix} follows the equilibrium potential difference $\Delta E^{eq,HCR}$ instead, in order to avoid large overpotentials η_{nt}^{HHCT}, as protons produced from H_2 CT could not be consumed rapidly by any other reaction. In case of "slow" defect incorporation, the current i_{nt}^{PCT} produced from PCT (Eq. 43) (orange line in Fig. 7) is negligible, since electrochemically produced or consumed polarons $O_O^{\bullet}$ can only be replaced through slow incorporation (Eq. 20). The difference between ΔE_{fast}^{mix} and ΔE_{slow}^{mix} (two red lines in Fig. 7) suggests that incorporation reactions indirectly have an influence on ΔE^{mix} due to defect concentration dependencies of CT reaction kinetics.

The thermodynamic extremes allow for a mixed cell potential between 0.854 V and 0.687 V for the given gas inlet and BCZYYb as electrolyte material. Based on Eq. 68, the difference of 0.167 V is related to the change in Gibbs energy obtained if the non-equilibrated fuel were to react to thermodynamic equilibrium.

In practice, the exchange current density $i_{nt}^{0,AHCT}$ for the ammonia-based CT reaction AHCT (Eq. 66) is expected to be small in comparison to $i_{nt}^{0,HHCT}$. In fact, many publications ignore the electrochemical activity of ammonia all together and assume ammonia formation or decomposition to be purely thermocatalytical,[78–80] thus suggesting ΔE^{mix} to be leaning toward the equilibrium potential difference $\Delta E^{eq,HCR} = 0.854$ V from Eq. 62. Figure 6 represents this qualitatively through a flat slope in the polarization curve for AHCT. Catalysts attractive for electrochemical ammonia synthesis are consequently expected to produce lower mixed cell potentials ΔE^{mix} in this context, since a lower mixed cell potential indicates a more favorable ratio between the limiting N_2 reduction kinetics and H_2 oxidation activity.

Alternative scenarios with relevance of mixed potentials are:

1. Ammonia-powered protonic ceramic fuel cells with locally incomplete NH_3 decomposition due to high fuel flow rates.[81–83] The quantitative impact of the AHCT reaction (Eq. 66) on ΔE^{mix}, determined by the ratio $i^{0,\text{AHCT}}/i^{0,\text{HHCT}}$ requires further investigation.
2. Potentiometric protonic ceramic hydrocarbon sensors for concentration quantification in the presence of multiple electrochemically active species.[84]
3. Catalyst activity screening experiments by relating a measured mixed potential directly to exchange current densities of active CT reactions on the catalyst[85,86] or by measuring mixed potentials of a gas phase before and after catalyst contact.[87,88]

In PCCs supplied with thermodynamically non-equilibrated fuels of known composition, ΔE^{mix} may serve as reference against measured cell potentials E_{OCV} at open-circuit conditions, in order to analyze the impact of leakage currents and potential drops across the cell.

Open Circuit Voltage

Contrary to the previous sections, which focused on the theoretical framework of equilibrium potentials in cells with multiple mobile charge carriers, this Section discusses the open-circuit voltage (OCV, E_{OCV}), which is the cell voltage at zero electric current flowing through the external circuit. It is explained why the open-circuit voltage is decreased compared to the thermodynamic equilibrium value for the reversible cell potential when multiple mobile charge carriers are present. It is further illustrated that electronic leakage currents are not the only cause for a decreased open-circuit voltage. The model used for calculating E_{OCV} suggests significant differences between equilibrium potentials $E^{\text{eq},r}$ for individual CT reactions at open-circuit (or polarized) cell conditions.

In order to measure a potential difference between two half cells, both half cells need to be connected electrically via an external circuit, as well as through an electrolyte as shown in Fig. 3, in order to close the overall charge and mass balance. In contrast to E_{rev}, which cannot be measured experimentally in cells with multiple mobile charge carriers, the open-circuit cell voltage E_{OCV} is measured at virtually zero electric current flowing through the external circuit. In consequence, no net current flows across the dense electrolyte either. In case of SCDC electrolytes, no defect fluxes are possible through the electrolyte at open circuit, as they could not be charge-balanced.[89] When using electrolytes with multiple mobile charge carriers however, the zero external current condition at open circuit merely demands the sum of charged fluxes through the dense electrolyte material to be zero:

$$\sum_{k \in \mathbf{S}_{\text{el}}} z_k J_k = 0, \qquad [87]$$

where $\mathbf{S}_{\text{el}}$ encompasses all species in the electrolyte material. J_k is the local flux of charged defect k. Thus, at open-circuit conditions individual defect fluxes can be non-zero and E_{OCV} cannot be defined through thermodynamics alone, i.e. it is dependent on kinetic parameters like defect mobility. These combined defect fluxes correspond to gas-permeation of the dense electrolyte membrane, as is the case for instance for a flow of $OH_O^{\bullet}$, which combined with a $V_O^{\bullet\bullet}$ flux in the opposing direction leads to H_2O crossover. Analogously a $OH_O^{\bullet}$ and $O_O^{\bullet}$ counterflow enable H_2 permeation.

PCC model.—A one-dimensional cell model that considers these kinetic processes is thus able to predict E_{OCV}. The model used here is adapted from Zhu, et al.[25] The flux J_k of charged defects can be estimated using the Nernst–Planck equation,[90] which includes diffusion and migration contributions and which is valid when assuming dilute solutions (i.e. no defect-defect interaction):

$$J_k = -D_k \nabla[X_k] - \frac{z_k F}{RT} D_k [X_k] \nabla \hat{\Phi}_{\text{el}}. \qquad [88]$$

$[X_k]$ is the local defect concentration and D_k its diffusion coefficient, which can be expressed through an Arrhenius approach[16] as

$$D_k = D_k^{\circ} \exp\left(-\frac{E_k}{RT}\right), \qquad [89]$$

with D_k° as pre-exponential factor and $E_{\text{act},k}$ as activation energy for species k. Values for BCZYYb are taken from[16] and given in Table II (without polaron trapping).

Table II. Kinetic parameters for defect diffusion coefficients in BCZYYb.[16]

Defect	D_k° [m^2/s]	$E_{\text{act},k}$ [kJ/mol]	D_k @ 500 °C [m^2/s]	D_k @ 700 °C [m^2/s]
$OH_O^{\bullet}$	1.09×10^{-7}	43.14	1.33×10^{-10}	5.27×10^{-10}
$V_O^{\bullet\bullet}$	1.87×10^{-7}	60.40	1.55×10^{-11}	1.07×10^{-10}
$O_O^{\bullet}$	2.19×10^{-5}	72.96	2.58×10^{-10}	2.66×10^{-09}

Within the model, local CT equilibrium potentials are calculated according to Eq. 15 for each CT reaction, since gas and defect fluxes lead to locally non-equilibrated species compositions. The following modifications are made in comparison to the model reported by Zhu, et al.,[25]

1. Thermodynamic data for BCZYYb has been taken from,[16] as given in Tables I and II.
2. Butler–Volmer equations for reactions HHCT (8) in the negatrode and OHCT (9) in the positrode were used as reported by Zhu, et al.,[25]

$$i^{\text{HHCT}} = i^{0,\text{HHCT}} \left[\exp\left(\frac{\beta_a F \eta^{\text{HHCT}}}{RT}\right) - \exp\left(-\frac{\beta_c F \eta^{\text{HHCT}}}{RT}\right) \right], \qquad [90]$$

however, introducing an Arrhenius dependency in the exchange current density $i^{0,r}$:

$$i^{0,\text{HHCT}} = i_0^{0,\text{HHCT}} \exp\left(-\frac{E_{\text{act}}^{\text{HHCT}}}{RT}\right) \times \frac{(p_{\text{H}_2}/p^*_{\text{H}_2})^{\beta_c/2}}{1 + (p_{\text{H}_2}/p^*_{\text{H}_2})^{1/2}} [\text{O}_\text{O}^{\text{x}}]^{\beta_c} [\text{OH}_\text{O}^{\bullet}]^{\beta_a}. \qquad [91]$$

The exchange current density $i^{0,r}$ and its prefactor $i_0^{0,r}$ should not be confused. The same Arrhenius formulation was introduced in OHCT (9):

$$i^{\text{OHCT}} = i^{0,\text{OHCT}} \left[\exp\left(\frac{\beta_a F \eta^{\text{OHCT}}}{RT}\right) - \exp\left(-\frac{\beta_c F \eta^{\text{OHCT}}}{RT}\right) \right], \qquad [92]$$

with

$$i^{0,\mathrm{OHCT}} = i_0^{0,\mathrm{OHCT}} \exp\left(-\frac{E_{\mathrm{act}}^{\mathrm{OHCT}}}{RT}\right) \times \frac{(p_{\mathrm{O_2}}/p_{\mathrm{O_2}}^*)^{(1/2-\beta_c/4)}(p_{\mathrm{H_2O}}/p_{\mathrm{H_2O}}^*)^{\beta_c/2}}{1+(p_{\mathrm{O_2}}/p_{\mathrm{O_2}}^*)^{1/2}+(p_{\mathrm{H_2O}}/p_{\mathrm{H_2O}}^*)} \times [\mathrm{O_O^x}]^{\beta_c}[\mathrm{OH_O^\bullet}]^{\beta_a}. \quad [93]$$

Exchange current density Arrhenius factors $i_0^{0,r}$ and E_{act}^r are treated as fit parameters. Defect concentrations are to be entered in mol/cm^3. β_a and β_c are symmetry factors. $p_{\mathrm{H_2}}$, $p_{\mathrm{O_2}}$ and $p_{\mathrm{H_2O}}$ are the local partial pressures, while $p_{\mathrm{H_2}}^*$, $p_{\mathrm{O_2}}^*$ and $p_{\mathrm{H_2O}}^*$ are calculated from the equilibrium constants $K_{\mathrm{ads,k}}$ for gas adsorption on the metal surface:[25]

$$p_k^* = 1/K_{\mathrm{ads},k}. \quad [94]$$

3. Polaron-charge-transfer (PCT, Eq. 43) is considered active in both half cells, represented through the mass-action law derived Butler–Volmer equation:

$$i^{\mathrm{PCT}} = i^{0,\mathrm{PCT}}\left[\exp\left(\frac{\beta_a F\eta^{\mathrm{PCT}}}{RT}\right) - \exp\left(-\frac{\beta_c F\eta^{\mathrm{PCT}}}{RT}\right)\right] \quad [95]$$

with:

$$i^{0,\mathrm{PCT}} = i_0^{0,\mathrm{PCT}} \exp\left(-\frac{E_{\mathrm{act}}^{\mathrm{PCT}}}{RT}\right)[\mathrm{O_O^x}]^{\beta_c}\,[\mathrm{O_O^\bullet}]^{\beta_a} \quad [96]$$

4. The model neglects the contribution from CT reactions H_2-vacancy-charge-transfer (HVCT, Eq. 1) and O_2-vacancy-charge-transfer (OVCT, Eq. 2) in congruence with literature. The assumption is justified due to low vacancy mobility (i.e., $D_{\mathrm{V_O^{\bullet\bullet}}}$) and it reduces the risk of over-parametrization of the model.
5. Equation 40 for strict local charge neutrality is replaced with the more general Poisson equation for electrostatics as

$$\nabla\cdot(\epsilon_0\epsilon_r\,\nabla\Phi_{\mathrm{el}}) = -\rho_{\mathrm{el}} = -\sum_{k\,\in\,\mathbf{S}_{\mathrm{el}}} z_k F[X_k], \quad [97]$$

where ϵ_0 and $\epsilon_r = 45.0$ (BZY10,[25]) are the vacuum and relative permittivity respectively, and ρ_{el} the local charge density in the electrolyte. Next to the positively charged mobile defects, the sum of charges includes the local concentrations of the negatively charged dopants yttrium and ytterbium, summed as $[\mathrm{X_B'}]$. Together with Eq. 88, this approach is called Nernst–Planck-Poisson model and includes a direct relation between the electrostatic potential in the electrolyte Φ_{el} and spatial defect distributions.

Defect concentration profiles $[X_k]$ in the dense electrolyte and the electrodes are dependent on defect fluxes J_k from Eq. 88), on source terms $\dot{s}_{\mathrm{V_O^{\bullet\bullet}}}$ (Eq. 32), $\dot{s}_{\mathrm{OH_O^\bullet}}$ (Eq. 33), $\dot{s}_{\mathrm{O_O^\bullet}}$ (34) and $\dot{s}_{\mathrm{O_O^x}}$ (35) from incorporation reactions HIR (20), OIR (Eq. 21), WIR (Eq. 22) and on CT reactions HHCT (Eq. 8), OHCT (Eq. 9) and PCT (Eq. 43). The gas phase composition in the porous electrode can be approximated using the Dusty Gas Model.[91–93] The cell model returns the local gas concentrations in the electrodes, the defect concentration profiles $[X_k]$, as well as electrostatic potential distributions Φ_{el} in the (porous) electrolyte and Φ_{ed} in the electron conducting phase as solution to the equation system for a given current density and inlet gas composition.

As E_{OCV} is dependent on kinetic parameters, model calibration includes polarized cell setpoints. Cell and operating parameters are given in Table III and charge transfer reaction parameters in Table IV with bold calibration parameters. Figure 8 shows a comparison between modeling and experimental results for an (air | porous BCZYYb+LSCF | dense BCZYYb | porous Ni-BCZYYb | fuel) fuel cell, using humidified H_2 (with locally equilibrated O_2) as fuel and humidified air (with locally equilibrated H_2) as oxidizer. Values are in good agreement at open circuit, as well as for the polarized cell.

Table III. Cell and operating parameters for BCZYYb+LSCF | BCZYYb | Ni-BCZYYb fuel cell, as tested in.[56] Since no thermodynamic and kinetic data for defects in LSCF is available, the LSCF fraction in the positrode is replaced with Ni in the model.

Parameter	Value	Unit
Negatrode:		
$H_2/H_2O/O_2$	97/3/equil.	mol%
Pressure	1	atm
Thickness	400	μm
Material	Ni+BCZYYb	
Volume ratio Ni/BCZYYb	0.45/0.55	m^3/m^3
Solid tortuosity	1.5	
Pore tortuosity	2	
Porosity	0.25	
Pore diameter	0.5	μm
Specific surface area defect incorp.	10^5	m^2/m^3
Positrode:		
$N_2/O_2/H_2O/H_2$	77/20/3/equil.	mol%
Pressure	1	atm
Thickness	33	μm
Material	Ni+BCZYYb	
Volume ratio Ni/BCZYYb	1/1	m^3/m^3
Solid tortuosity	1.6	
Pore tortuosity	2	
Porosity	0.25	
Pore diameter	0.5	μm
Specific surface area defect incorp.	10^5	m^2/m^3
Dense electrolyte:		
Thickness	14	μm
Material	BCZYYb	
General:		
Defect thermodynamics	BCZYYb (Table I)	
Defect diffusion coefficients	BCZYYb (Table II)	
Incorporation forward rate constants	BZY10[60]	

For further validation of the parameters given in Table IV, an LSCF | BCZYYb | Ni-BCZYYb cell was manufactured considering cell parameters in Table III and E_{OCV} measured at different air inlet humidities. Variation of humidity at open circuit had not been part of the model calibration process. The measured values of E_{OCV} are compared against the model prediction in Fig. 9, showing good agreement. Figure 9 also shows the two gas-phase based Nernst potentials $E_{\mathrm{Nernst(gas)}}^{\mathrm{HCR}}$ and $E_{\mathrm{Nernst(gas)}}^{\mathrm{V\,CR}}$, as well as the reversible cell potential E_{rev}. As can be seen, $E_{\mathrm{Nernst(gas)}}^{\mathrm{HCR}}$ can be a good approximation for E_{rev} when the gases supplied to the half cells are both reasonably humid.

The ambiguity between $E_{\mathrm{Nernst(gas)}}^{\mathrm{V\,CR}}$ and $E_{\mathrm{Nernst(gas)}}^{\mathrm{HCR}}$ is further emphasized in Fig. 9. As can be seen in both Figs. 8 and 9, E_{OCV} is significantly below E_{rev} for all temperatures and humidities, indicated as "potential drop" in the enlargement of Fig. 8.

OCV case study.—This Section studies the origin of the potential drop (i.e. difference between E_{rev} and E_{OCV}) in a case study based on the conditions and parameters given in Tables III and IV at an operating temperature of 600 °C (black dashed arrow in Fig. 8).

Figure 10a illustrates the 1-dimensional potential distributions throughout the button cell at E_{OCV}, including the potential drop.

Table IV. Charge transfer reaction parameters. Model calibration parameters are bold. "Sensitivity" refers to the relative change in cell current density at 600 °C and 0.7 V when increasing the parameter value by +5%. β values were increased by +0.05 instead of +5% and $\beta_a + \beta_c = 1$ was maintained.

Parameter	Value	Unit	Sensitivity
Negatrode:			
HHCT (Eq. 8):			
β_a	**0.9**		−1.4%
β_c	**0.1**		+1.5%
$i_0^{0,\mathrm{HHCT}}$	**5.25×10^{12}**	**A/cm^3**	+1.1%
$E_{\mathrm{act,nt}}^{\mathrm{HHCT}}$	**134.5**	**kJ/mol**	−20.7%
$K_{\mathrm{ads,H_2}}$	70		
PCT (Eq. 43):			
β_a	**0.5**		+0.004%
β_c	**0.5**		−0.004%
$i_0^{0,\mathrm{PCT}}$	**1.58×10^{8}**	**A/cm^3**	−0.001%
$E_{\mathrm{act,nt}}^{\mathrm{PCT}}$	0.0	kJ/mol	
Positrode:			
OHCT (Eq. 9):			
β_a	**0.23**		−3.2%
β_c	**0.77**		+3.0%
$i_0^{0,\mathrm{OHCT}}$	**1.11×10^{13}**	**A/cm^3**	+0.6%
$E_{\mathrm{act}}^{\mathrm{OHCT}}$	**134.5**	kJ/mol	−12.7%
$K_{\mathrm{ads,H_2O}}$	**2282**		−0.3%
$K_{\mathrm{ads,O_2}}$	70		
PCT (Eq. 43):	See negatrode		

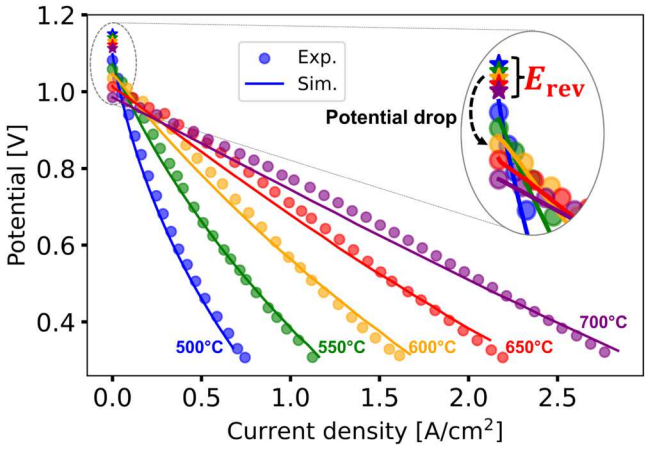

Figure 8. Experimental and simulated IV-data for a BCZYYb-LSCF | BCZYYb | Ni-BCZYYb fuel cell supplied with H_2 and air —both humidified to 3 mol% H_2O content and an operating pressure of 1 atm. Experimental, cell and simulation parameters are given in Tables III and IV. The potential drop indicates the difference between E_{rev} and E_{OCV}. Experimental data from.[56]

Dotted lines in Fig. 10a show the positions which electrostatic potentials would assume in case of thermodynamic equilibrium of all reactions, in absence of an electrolyte membrane between the electrodes. The enlargement Fig. 10b suggests that the potential drop is due to overpotentials in the electrodes (white background) and in the dense electrolyte membrane (gray background), leading to a gradient in the electrostatic potential $\hat{\Phi}_{\mathrm{el}}$. The dotted lines in Fig. 10b are slightly curved due to local gas composition variations, changing the local values for CT equilibrium potentials $\hat{E}_{\mathrm{nt}}^{\mathrm{eq,HHCT}}$ and

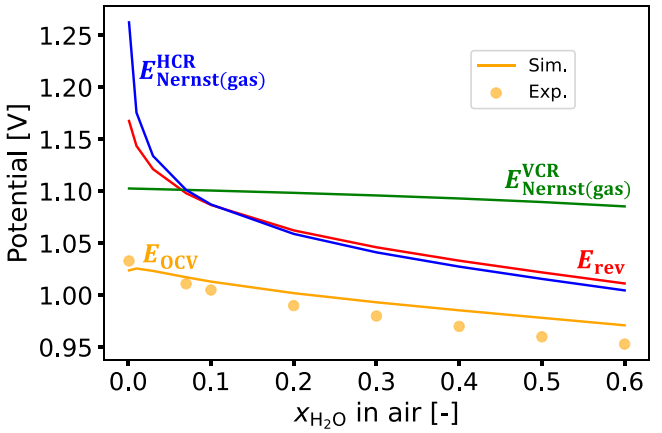

Figure 9. Simulated and measured E_{OCV} at increasing humidity of air in the positrode inlet. Negatrode gas inlet contains 7 mol% H_2O in H_2 fuel. Trace H_2 and O_2 are calculated according to WFR equilibrium for positrode and negatrode respectively. E_{OCV} is simulated based on model parameters from Tables III and IV.

$\hat{E}_{\mathrm{Pt}}^{\mathrm{eq,OHCT}}$, thus indicating minor concentration overpotentials at open circuit.

The potential drop in the dense electrolyte (black arrow in Fig. 10) results from the net zero charge flux requirement (87) in the dense electrolyte at open-circuit conditions. According to the Nernst–Planck equation (Eq. 88), defect concentration differences between electrodes (Fig. 13) are a driving force for diffusion fluxes. These diffusion fluxes through the electrolyte don't balance to a sum of zero current through concentration gradients alone. Instead, overall charge flux balance is achieved through an electrostatic potential gradient in the dense electrolyte, leading to a migration contribution in the flux of each defect and a contribution to the drop in the cell voltage. Figure 11 shows the resulting defect fluxes in opposing directions, leading to a net zero charge flux. Polaron ($O_O^{\bullet}$) defect fluxes in the dense electrolyte, typically associated with electronic leakage, contribute significantly to the open-circuit cell voltage potential drop, as can be seen in Fig. 11. In fact, at 600 °C and open circuit conditions the average transference numbers for the three defects in the dense electrolyte are $t_{\mathrm{OH_O^{\bullet}}} = 0.85$, $t_{\mathrm{V_O^{\bullet\bullet}}} = 0.07$ and $t_{\mathrm{O_O^{\bullet}}} = 0.08$, underlining the presence of mobile polarons. The transference number values result from the model structure and parameters given in Tables III and IV.

This process producing gradients in the electrostatic potential of the electrolyte was originally described by Wagner in 1933 in corrosion science for a metal surface corroding in an oxidizing gas atmosphere.[94] The potential drop was termed "diffusion potential" by Wagner based on defect diffusion during metal corrosion, but may be termed "diffusion leakage overpotential" $\eta^{\mathrm{Diff.}}$ in the context of fuel or electrolysis cells, in order to avoid confusion with overpotentials related to gas diffusion limitations in the porous electrodes (also called concentration overpotentials[95]).

Larger than the diffusion leakage overpotential $\eta^{\mathrm{Diff.}}$ are the potential drops in the electrodes. As suggested in Fig. 10b in brown, the potential drops in the electrodes result from activation overpotentials, whereby multiple CT reactions in each electrode lead to net-zero current production. The overpotential distribution in the electrodes is dependent on CT kinetics and defect mobility in the porous electrolyte. $OH_O^{\bullet}$ are produced and consumed via CT reactions HHCT (Eq. 8) and OHCT (Eq. 9) over a wider range in the electrodes, while the charge production is compensated by $O_O^{\bullet}$ consumption and production through CT reaction PCT (Eq. 43) very close to the dense electrolyte. The electrochemical reactions lead to a consumption of H_2 and O_2 and a production of H_2O at open circuit, lowering faradaic efficiencies of PCCs when operated close to open

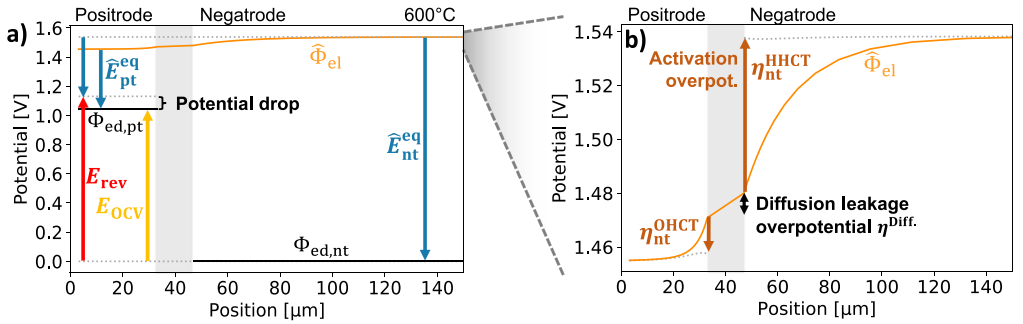

Figure 10. Simulated spatial potential drop across cell at open-circuit conditions, 600 °C and 3 mol% H_2O in H_2 fuel, as well as in air. Figure b) shows the enlarged electrolyte potential profile with the activation overpotentials in brown for reactions HHCT (8) and OHCT (9) in negatrode and positrode respectively as well as an overpotential in the dense electrolyte (black). For better visibility only parts of the negatrode thickness are shown. Concentration overpotentials at open circuit are minimal.

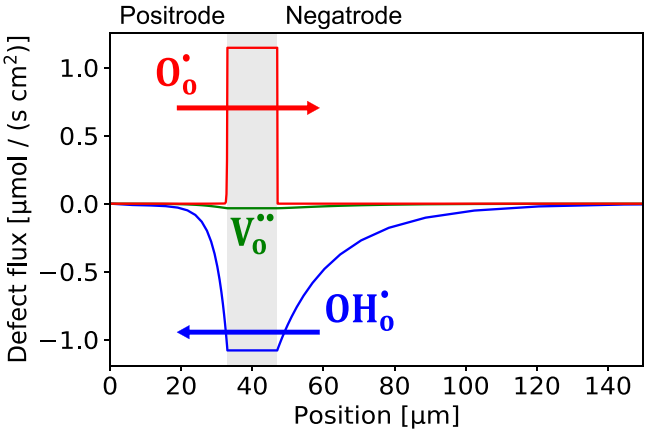

Figure 11. Defect fluxes equilibrate the charge balance in the dense electrolyte at open-circuit conditions. Simulated at 600 °C with 3 mol% H_2O in both H_2 fuel and air.

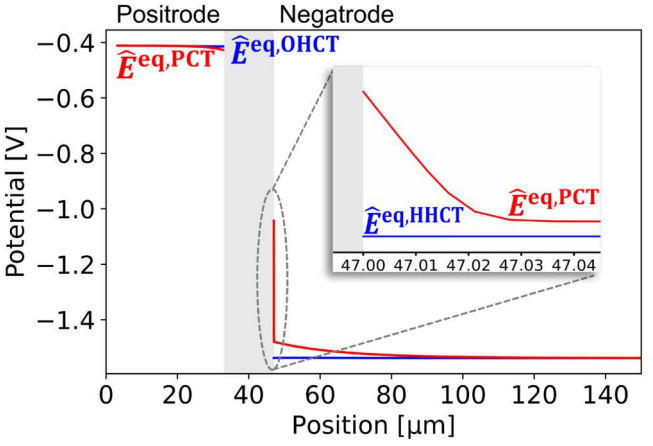

Figure 12. Local CT equilibrium potentials for reactions HHCT (Eq. 8), OHCT (Eq. 9) and PCT (Eq. 43) at open-circuit conditions at 600 °C with 3 mol% humidified H_2 and 3 mol% humidified air supply.

circuit.[45] Activation overpotentials of individual CT reactions differ within the same electrode since their respective CT equilibrium potentials diverge locally, as shown in Figure 12.

Due to defect fluxes across the dense electrolyte, the local defect concentrations in the electrodes are not in equilibrium with the gas phase, leading to diverging CT equilibrium potentials: $E_{nt}^{eq,HHCT} \neq E_{nt}^{eq,PCT}$ and $E_{pt}^{eq,OHCT} \neq E_{pt}^{eq,PCT}$. As shown in the enlargement of Fig. 12, this is especially true for $E_{nt}^{eq,PCT}$ (red line) in

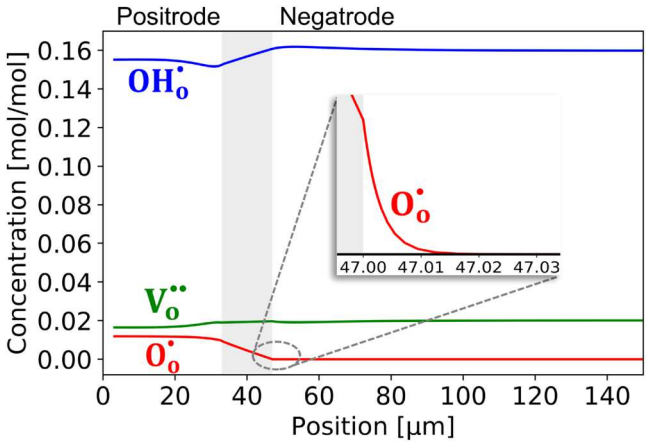

Figure 13. Spatial defect concentrations at open-circuit conditions and 600 °C. 3 mol% humidified H_2 and 3 mol% humidified air. Enlargement: Polarons $O_O^{\bullet}$ spill from the dense electrolyte into the negatrode due to concentration gradients, leading to elevated concentrations.

the negatrode, due to the spill-over of polarons from the dense electrolyte, leading to elevated $O_O^{\bullet}$ concentrations in the negatrode close to the membrane, as shown in Fig. 13.

The CT equilibrium potential $E_{nt}^{eq,PCT}$ drops close to the dense electrolyte in the negatrode, until the largest excess of polarons $O_O^{\bullet}$ from spill-over is consumed through CT reaction PCT (43). This happens in a very narrow range, as the PCT is considered to be comparatively fast, since no gas species bond-splitting is involved. (For instance, close to the dense electrolyte the exchange current density for PCT is $i^{0,PCT} = 11596\ A/cm^3$, while for the HHCT reaction it is $i^{0,HHCT} = 66\ A/cm^3$). $E_{nt}^{eq,PCT}$ remains slightly elevated compared to $E_{nt}^{eq,HHCT}$ in blue, up until cell position coordinate 100 μm. The reason is an excess of protons $OH_O^{\bullet}$ originating from CT reaction HHCT (8), which are converted back to polarons $O_O^{\bullet}$ through defect chemistry reaction HIR (20). Consequently, the local polaron concentration is slightly above the thermodynamic equilibrium concentration defined by the gas phase composition, thus elevating $E_{nt}^{eq,PCT}$.

The phenomenon of overpotentials in the electrode at open-circuit conditions is limited to cells with multiple mobile charge carriers, since in SCDC cells do not allow for defect fluxes across the dense electrolyte in this case. Potential drops due to activation overpotentials at open circuit are in accordance with experiments conducted by Sumi et al., who recently estimated the magnitude of activation overpotentials based on electrochemical impedance spectroscopy measurements and distribution of relaxation time analysis conducted on a BCZYYb-based cell at 600 °C.[18] Their work showed

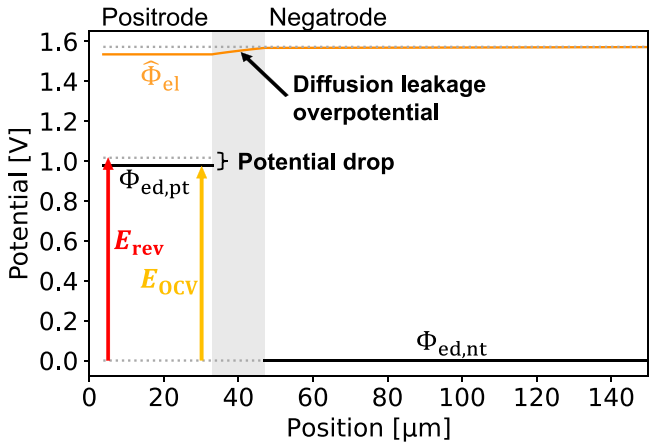

Figure 14. Simulated spatial potential drop at open-circuit conditions for a cell with two mobile charge carriers but without a charge carrier associated with electronic leakage. 0.5 mol% H_2O in H_2 fuel, and 90 mol% H_2O in air at 600 °C. Considering only $OH_O^{\bullet}$ and $V_O^{\bullet\bullet}$.

that overpotentials in the electrodes could in fact have a higher contribution to the total potential drop than potential differences across the dense electrolyte. The result is further supported by findings of Shimada et al. who experimentally identified electrode polarization resistances as relevant factor for decreased E_{OCV}.[24]

Hypothetical scenario.—It can be shown on a theoretical basis that a potential drop exists (i.e. $E_{OCV} \neq E_{rev}$), even when there are no defects associated with electronic leakage current (like free electrons e', electron holes $h^{\bullet}$ or polarons $O_O^{\bullet}$), thus only considering $OH_O^{\bullet}$ and $V_O^{\bullet\bullet}$ as mobile defects.

$OH_O^{\bullet}$ and $V_O^{\bullet\bullet}$ are produced and consumed through the defect incorporation reaction WIR (22), which is assumed here to be very fast, i.e. equilibrated. Charge transfer reactions HHCT (8) and OHCT (9) are reversible, while reaction PCT (43) is not possible, since no polarons $O_O^{\bullet}$ shall be present. Additionally, the gas composition is changed to enhance the potential drop originating from humidity differences: A negatrode fuel gas composition of 0.5 mol% H_2O in H_2 (equilibrated with O_2) is considered, while the positrode supply consists of highly humidified air, i.e. 90 mol% H_2O, 2.1 mol% O_2, (equilibrated with H_2) with N_2 covering the remains. Figure 14 illustrates the potential drop in the dense electrolyte for this hypothetical scenario.

Diffusion fluxes of charged $OH_O^{\bullet}$ and $V_O^{\bullet\bullet}$ in the dense electrolyte are countered with an electrostatic gradient to fulfill Eq. 87 in the dense electrolyte. To achieve a gradient in $\hat{\Phi}_{el}$ half cell potentials are shifted against each other, leading to a lowered E_{OCV} compared to E_{rev}. Thus, electronic leakage is technically not required for lowered E_{OCV}, instead a potential drop can be an intrinsic consequence of electrolyte materials which are able to conduct more than one mobile charge carrier. The driving force for the described defect fluxes is largely the partial pressure difference of water between the two half cells. In total, these considerations highlight that in cells with multiple mobile charge carriers E_{OCV} is defined not only by thermodynamics, but also kinetics and material properties.

Analytical equation for OCV.—For the analysis of systems such as potentiometric sensors based on protonic ceramic materials, being able to calculate the open-circuit voltage is critical.[8] As formulating a 1-dimensional model based on multiple differential equations can be cumbersome, an analytical equation may be used instead, which is based on the assumption of reversible, interfacial electrodes (i.e. infinitely high exchange current densities and defect incorporation rates without gas transport phenomena).[38–41,42] Thus, activation and concentration overpotentials are not considered:

$$E_{OCV,ana.} = \frac{RT}{F}\int_0^L \left\{ \frac{t_{OH_O^{\bullet}}(x)}{2} \frac{d\left(\ln\left(\frac{p_{H_2O}(x)}{p^{\circ}}\right)\right)}{dx} - \frac{t_{OH_O^{\bullet}}(x) + t_{V_O^{\bullet\bullet}}(x)}{4} \frac{d\left(\ln\left(\frac{p_{O_2}(x)}{p^{\circ}}\right)\right)}{dx} \right\} dx, \quad [98]$$

with $x = 0$ being the bulk-air-compartment/porous-electrode interface coordinate and $x = L$ the porous-electrode/bulk-fuel-compartment interface. Its derivation traces back to Wagner.[94] The analytical calculation of $E_{OCV,ana.}$ relies on spatial defect transference number profiles $t_k(x)$:[39]

$$t_k(x) = \frac{\sigma_k(x)}{\sum_k \sigma_k(x)}, \quad [99]$$

where $\sigma_k(x)$ is the defect conductivity related to the spatial defect concentration profile $[X_k]$ and the diffusion coefficient D_k from Eq. 89 through

$$\sigma_k(x) = \frac{(z_k F)^2}{RT} D_k\,[X_k]. \quad [100]$$

According to Eq. 98, calculation of $E_{OCV,ana.}$ requires $p_{H_2O}(x)$ and $p_{O_2}(x)$ not only at the electrode/electrolyte interfaces, but also in the dense electrolyte where no gas is present. Partial pressures can instead be calculated based on local defect concentrations using the equilibrium constants $K_{p,WIR}$ and $K_{p,OIR}$.

For example, using the model parameters from Tables III and IV, while significantly decreasing the electrode extension and increasing exchange current density pre-factors and defect incorporation rate constants (reversible interfacial electrode), the open-circuit voltage at 600 °C and 3 mol% humidity in air and fuel calculates as $E_{OCV} = E_{OCV,ana.} = 1.1127$ V by both the differential equation system and the analytical Eq. 98, proving consistency of the approaches. (For comparison, $E_{rev} = 1.1312$ V). For the calculation of $E_{OCV,ana.}$ spatial defect concentration profiles $[X_k]$ were taken from the solution of the numeric equation system. Since the transference number profiles in the dense electrolyte $t_k(x)$ are not spatially invariant, a rigorous calculation of $E_{OCV,ana.}$ requires solving a path-dependent integral.[40] In an effort to simplify the calculation further, one might instead assume spatially invariant, averaged values for $t_k(x)$ (possibly extracted from experiments), which transforms the integral into a simple algebraic equation,[38]

$$E_{OCV,ana.}^{simple} = \frac{RT}{F}\frac{t_{OH_O^{\bullet}}}{2}\ln\left(\frac{p_{H_2O}(L)}{p_{H_2O}(0)}\right) - \frac{RT}{F}\frac{t_{OH_O^{\bullet}} + t_{V_O^{\bullet\bullet}}}{4}\ln\left(\frac{p_{O_2}(L)}{p_{O_2}(0)}\right). \quad [101]$$

This also alleviates the need for knowledge of thermodynamic parameters, such as for $K_{p,WIR}$ and $K_{p,OIR}$ for the calculation of $p_{H_2O}(x)$ and $p_{O_2}(x)$ inside the dense electrolyte. Therefore, Eq. 101 allows for direct approximation of the OCV, under the assumption of reversible interfacial electrode processes and spatially averaged transference numbers. For the given scenario $E_{OCV,ana.}^{simple} = 1.0190$ V. To predict E_{OCV} accurately with fewer restrictive assumptions, a numerical model as presented herein remains essential for systems containing multiple mobile charge carriers.

Conclusions

This work presents a fundamental framework for evaluating equilibrium potentials in electrochemical systems utilizing an electrolyte material capable of conducting multiple charge carriers. A distinction between reversible cell potentials, as determined from thermodynamics, and cell potentials that are experimentally measured is drawn. With regard to reversible cell potential, it is demonstrated that commonly used gas-phase based Nernst equation does not accurately capture the thermodynamic driving forces in cells with multiple mobile charge carriers. Instead, the reversible cell potential should be calculated according to Eq. 18 using two half-cell equilibrium potentials given by Eq. 15. These half-cell equilibrium potentials include the species activities of mobile defects created or consumed by the charge transfer reactions. This ensures that the potential energy contribution of concentration differences of mobile charge carriers across the electrolyte membrane are considered in the reversible cell potential, as illustrated exemplarily by equations Equation 62, Eq. 63 and Eq. 64 which can be used interchangeably to calculate the reversible cell potential of a PCC supplied with humidified H_2 and air.

It is shown that equilibrium potentials derived from various charge transfer reactions coincide when all species are thermodynamically equilibrated within each half cell, thus leading to a well-defined reversible cell potential. Conversely, when the gas supply to a half-cell is not thermodynamically equilibrated, equilibrium potentials associated with individual charge transfer reactions diverge and a well-defined reversible cell potential does not exist. Instead, mixed-potential theory can be utilized for the calculation of a theoretical steady-state cell potential in this scenario. It is demonstrated that the resulting mixed cell potential is dependent on kinetics, including influences of defect reactions and cannot be derived from thermodynamics alone. Its value falls between the reversible cell potentials that would be obtained if each fuel species in the mixture were present alone as the sole active component. The main deciding factor for the exact value of the mixed cell potential is the ratio of exchange current densities of the competing charge transfer reactions.

With regards to measurable cell potentials, a parameterized model for a protonic ceramic cell is used to highlight spatially distributed processes occurring in the electrodes and dense electrolyte at open-circuit conditions. It is shown that the difference between measured and reversible potential can be explained by a potential drop in the dense electrolyte, as well as activation overpotentials in non-reversible electrodes. Furthermore, it is shown that potential drops can occur even if no charge carriers like electron holes or polarons (which are typically associated with electronic leakage currents) are present. Summarizing, a multitude of factors lead to deviations between gas-phase based Nernst predictions and cell potentials measured at open-circuit conditions in cells with multiple mobile charge carriers: defect-based Nernst potential contributions, non-equilibrated inlet gas mixtures, activation overpotentials, electronic leakage currents and ionic defect fluxes may be present.

The following practical conclusions can be drawn from this work:

1. Accurately determining equilibrium potentials and open-circuit voltages in systems with multiple mobile charge carriers requires detailed knowledge of the relevant thermodynamic and kinetic defect parameters, highlighting the need for further research across a wider range of materials.
2. When thermodynamic data of the electrolyte is unavailable and the inlet gases are thermodynamically equilibrated, it is still recommended to derive the equation for the reversible potential according to Eq. 18 with the half-cell equilibrium potentials Eq. 15, instead of using a purely gas-phase based Nernst equation. This facilitates an educated guess on the influence of mobile charge carrier concentration differences on the reversible cell potential. In the present study on PCCs, it was found that differences in water vapor partial pressure between the electrodes exacerbate the deviation between the commonly used gas-phase based Nernst equation and the true reversible cell potential.
3. In modeling studies accounting for spatially distributed electrode processes or thermodynamically nonequilibrated gas supply, the use of locally evaluated charge transfer equilibrium potentials for each individual reaction is essential. They can be calculated according to Eq. 15 based on local gas and defect compositions. Equilibrium potentials for different charge transfer reactions diverge during operation as a result of local nonequilibrium conditions, and neglecting this differentiation will lead to inaccuracies in the predicted electrochemical behavior.
4. Proper OCV calculation necessitates numerical methods. However, simplified algebraic expressions such as Eq. 101 based on averaged transference numbers of mobile defects may serve as a practical approximation.

Acknowledgments

The research work presented herein was funded by the Deutsche Forschungsgemeinschaft within the NSF-DFG Echem initiative, project number 460038541. We further thank the Karlsruhe House of Young Scientists (KHYS) for funding of a research visit at Colorado School of Mines.

ORCID

Felix Ehrlich https://orcid.org/0009-0007-3236-3825
Akhil Ashar https://orcid.org/0009-0007-4240-3341
Oscar Furst https://orcid.org/0009-0007-7772-3660
Philipp Blanck https://orcid.org/0009-0000-3683-2704
Huayang Zhu https://orcid.org/0009-0005-4056-4569
Robert J. Braun https://orcid.org/0000-0001-5319-3350
Robert J. Kee https://orcid.org/0000-0003-3930-4784
Olaf Deutschmann https://orcid.org/0000-0001-9211-7529

References

1. R. P. O'Hayre, S.-W. Cha, W. G. Colella, and F. B. Prinz, *Fuel Cell Fundamentals* (Wiley, Hoboken, NJ) 3rd ed. (2016).
2. P. Cavaliere, *Water Electrolysis for Hydrogen Production* (Springer Nature Switzerland AG, Berlin) 1st ed. (2023).
3. A. Rao, J. Maclay, and S. Samuelsen, "Efficiency of electrochemical systems." *J. Power Sources*, **134**, 181 (2004).
4. H. Zhu and R. J. Kee, "Thermodynamics of SOFC efficiency and fuel utilization as functions of fuel mixtures and operating conditions." *J. Power Sources*, **161**, 957 (2006).
5. K. Li, T. Murakami, Y. Nagata, Y. Mikami, K. Yamauchi, T. Kuroha, Y. Okuyama, Y. Mizutani, M. Mori, and T. Araki, "What kind of PCFC material physical property values do we need?—From a system efficiency perspective." *Appl. Energy*, **381**, 125132 (2025).
6. X. Huang, J. Shi, Z. Liu, Y. Wang, X. Ye, and Y. Shi, "Numerical study on current leakage of a tubular protonic ceramic fuel cell." *J. Power Sources*, **631**, 236241 (2025).
7. J. Bobacka, A. Ivaska, and A. Lewenstam, "Potentiometric ion sensors." *Chem. Rev.*, **108**, 329 (2008).
8. A. Volkov, E. Gorbova, A. Vylkov, D. Medvedev, A. Demin, and P. Tsiakaras, "Design and applications of potentiometric sensors based on proton-conducting ceramic materials. A brief review." *Sens. Actuators B: Chem.*, **244**, 1004 (2017).
9. H. Shimada et al., "Protonic ceramic fuel cell with bi-layered structure of $BaZr_{0.1}Ce_{0.7}Y_{0.1}Yb_{0.1}O_{3-\delta}$ functional interlayer and $BaZr_{0.8}Yb_{0.2}O_{3-\delta}$ electrolyte." *J. Electrochem. Soc.*, **168**, 124504 (2021).
10. X. Wang, M. Han, Y. Huang, Y. Zhang, B. Ma, Q. Zhou, K. Sun, and H. Zhong, "Influences of the thickness and density of the gadolinia doped ceria barrier layer on the performance of the solid oxide fuel cell." *Int. J. Hydrogen Energy*, **113**, 355 (2025).
11. W. Bessler, J. Warnatz, and D. Goodwin, "The influence of equilibrium potential on the hydrogen oxidation kinetics of SOFC anodes." *Solid State Ionics*, **177**, 3371 (2007).
12. D. P. Xenos, P. Hofmann, K. D. Panopoulos, and E. Kakaras, "Detailed transient thermal simulation of a planar SOFC (solid oxide fuel cell) using gPROMS^{TM}." *Energy*, **81**, 84 (2015).
13. J.-C. Njodzefon, D. Klotz, A. Kromp, A. Weber, and E. Ivers-Tiffée, "Electrochemical modeling of the current-voltage characteristics of an SOFC in fuel cell and electrolyzer operation modes." *J. Electrochem. Soc.*, **160**, F313 (2013).

14. M. Andersson, J. Yuan, and B. Sundn, "SOFC modeling considering electrochemical reactions at the active three phase boundaries." *Int. J. Heat Mass Transf.*, **55**, 773 (2012).
15. D. Bhattacharyya and R. Rengaswamy, "A review of solid oxide fuel cell (SOFC) dynamic models." *Ind. Eng. Chem. Res.*, **48**, 6068 (2009).
16. H. Zhu, S. Ricote, C. Duan, R. P. O'Hayre, and R. J. Kee, "Defect chemistry and transport within dense $BaCe_{0.7}Zr_{0.1}Y_{0.1}Yb_{0.1}O_{3-\delta}$ (BCZYYb) proton-conducting membranes." *J. Electrochem. Soc.*, **165**, F845 (2018).
17. Z. Li, J. Yu, C. Wang, I. T. Bello, N. Yu, X. Chen, K. Zheng, M. Han, and M. Ni, "Multi-objective optimization of protonic ceramic electrolysis cells based on a deep neural network surrogate model." *Appl. Energy*, **365**, 123236 (2024).
18. H. Sumi et al., "Investigation of degradation mechanisms by overpotential evaluation for protonic ceramic fuel cells." *J. Power Sources*, **582**, 233528 (2023).
19. R. Qiu et al., "Multifactor theoretical analysis of current leakage in proton-conducting solid oxide fuel cells." *J. Power Sources*, **505**, 230038 (2021).
20. J.-H. Zhang, L.-B. Lei, D. Liu, F.-Y. Zhao, M. Ni, and F. Chen, "Mathematical modeling of a proton-conducting solid oxide fuel cell with current leakage." *J. Power Sources*, **400**, 333 (2018).
21. C. Wang, Z. Li, S. Zhao, L. Xia, M. Zhu, M. Han, and M. Ni, "Modelling of an integrated protonic ceramic electrolyzer cell (PCEC) for methanol synthesis." *J. Power Sources*, **559**, 232667 (2023).
22. I. Zvonareva, X.-Z. Fu, D. Medvedev, and Z. Shao, "Electrochemistry and energy conversion features of protonic ceramic cells with mixed ionic-electronic electrolytes." *Energy Environ. Sci.*, **15**, 439 (2022).
23. K. J. Albrecht, A. Dubois, K. Ferguson, C. Duan, R. P. O'Hayre, and R. J. Braun, "Steady-state and dynamic modeling of intermediate-temperature protonic ceramic fuel cells." *J. Electrochem. Soc.*, **166**, F687 (2019).
24. H. Shimada, T. Yamaguchi, H. Sumi, Y. Yamaguchi, K. Nomura, Y. Mizutani, and Y. Fujishiro, "A key for achieving higher open-circuit voltage in protonic ceramic fuel cells: lowering interfacial electrode polarization." *ACS Appl. Energy Mater.*, **2**, 587 (2019).
25. H. Zhu and R. J. Kee, "Modeling protonic-ceramic fuel cells with porous composite electrodes in a button-cell configuration." *J. Electrochem. Soc.*, **164**, F1400 (2017).
26. H. Zhu and R. J. Kee, "Membrane polarization in mixed-conducting ceramic fuel cells and electrolyzers." *Int. J. Hydrogen Energy*, **41**, 2931 (2016).
27. H. Zhu, B. M. Blackburn, R. Wang, M. A. Kelly, A. Hack, S. Reinartz, G. S. Jackson, and R. J. Kee, "Modeling a high-temperature electrochemically driven water-gas-shift process using a mixed-conducting membrane without external electrical power." *J. Electrochem. Soc.*, **172**, 044513 (2025).
28. H. Zhu, A. Ashar, R. J. Kee, R. J. Braun, and G. S. Jackson, "Physics-based model to represent membrane-electrode assemblies of solid-oxide fuel cells based on gadolinium-doped ceria." *J. Electrochem. Soc.*, **170**, 104506 (2023).
29. K. Li, T. Araki, T. Kawamura, A. Ota, and Y. Okuyama, "Numerical analysis of current efficiency distributions in a protonic ceramic fuel cell using Nernst-Planck-Poisson model." *Int. J. Hydrogen Energy*, **45**, 34139 (2020).
30. J. Zhu, H. Zhu, H. Zhu, Y. Han, Z. Li, B. Chen, Y. Zhang, P. Zhu, M. Ni, and H. Xu, "How can current leakage be reduced in protonic ceramic electrolysis cells? Insights from thermo-electrochemical modeling." *J. Power Sources*, **642**, 236957 (2025).
31. R. J. Kee, S. Ricote, H. Zhu, R. J. Braun, G. Carins, and J. E. Persky, "Perspectives on technical challenges and scaling considerations for tubular protonic-ceramic electrolysis cells and stacks." *J. Electrochem. Soc.*, **169**, 054525 (2022).
32. H. Zhu, S. Ricote, and R. J. Kee, "Thermodynamics, transport, and electrochemistry in protonic-ceramic electrolysis cells." *High Temperature Electrolysis, from Fundamentals to Applications*, ed. W. Sitte and R. Merkle (IOP publishing, Bristol, UK) 12–11 (2022).
33. M. Okazaki and J. Otomo, "Electrode-supported protonic ceramic electrolysis cells for electrochemically promoted ammonia synthesis at intermediate temperatures." *ACS Omega*, **8**, 40299 (2023).
34. Q. Hu, C. Tian, D. Bao, H. Zhong, and X. Zhang, "Protonic ceramic electrochemical cells: opportunities and challenges for ammonia synthesis." *Next Energy*, **4**, 100144 (2024).
35. Y. Wang, Y. Ling, B. Wang, G. Zhai, G. Yang, Z. Shao, R. Xiao, and T. Li, "A review of progress in proton ceramic electrochemical cells: material and structural design, coupled with value-added chemical production." *Energy Environ. Sci.*, **16**, 5721 (2023).
36. C. Duan, R. J. Kee, H. Zhu, N. Sullivan, L. Zhu, L. Bian, D. Jennings, and R. P. O'Hayre, "Highly efficient reversible protonic ceramic electrochemical cells for power generation and fuel production." *Nat. Energy*, **4**, 230 (2019).
37. Y. Wang, H. Zhang, J. Cao, K. Xu, K. Pei, and Y. Chen, "Highly selective reduction of CO_2 through a protonic ceramic electrochemical cell." *J. Power Sources*, **524**, 231101 (2022).
38. T. Norby and P. Kofstad, "Proton and native-ion conductivities in Y_2O_3 at high temperatures." *Solid State Ionics*, **20**, 169 (1986).
39. L. Heyne, "Electrochemistry of mixed ionic-electronic conductors." *Solid Electrolytes, Topics in Applied Physics*, ed. S. Geller (Springer-Verlag, Heidelberg)192 (1977).
40. H.-I. Yoo and M. Martin, "On the path-dependence of the open-cell voltage of a galvanic cell involving a ternary or multinary compound with multiple mobile ionic species under multiple chemical potential gradients." *Phys. Chem. Chem. Phys.*, **12**, 14699 (2010).
41. N. S. Choudhury and J. W. Patterson, "Performance characteristics of solid electrolytes under steady-state conditions." *J. Electrochem. Soc.*, **118**, 1398 (1971).
42. H.-I. Ji, H. Kim, H.-W. Lee, B.-K. Kim, J.-W. Son, K. J. Yoon, and J.-H. Lee, "Open-cell voltage and electrical conductivity of a protonic ceramic electrolyte under two chemical potential gradients." *Phys. Chem. Chem. Phys.*, **20**, 14997 (2018).
43. Q. Zhang, Y. Guo, and J. Ding, "Characterization of the conductivity distribution and leakage current in proton-conducting ceramic electrolyte through modeling and sensitivity analysis." *Int. J. Hydrogen Energy*, **46**, 31370 (2021).
44. H. Sumi, H. Shimada, Y. Yamaguch, Y. Mizutani, Y. Okuyama, and K. Amezawa, "Comparison of electrochemical impedance spectra for electrolyte-supported solid oxide fuel cells (SOFCs) and protonic ceramic fuel cells (PCFCs)." *Sci. Rep.*, **11**, 10622 (2021).
45. H. Zhu, S. Ricote, and R. J. Kee, "Faradaic efficiency in protonic-ceramic electrolysis cells." *J. Phys. Energy*, **4**, 014002 (2022).
46. S. Choi, T. C. Davenport, and S. M. Haile, "Protonic ceramic electrochemical cells for hydrogen production and electricity generation: exceptional reversibility, stability, and demonstrated faradaic efficiency." *Energy Environ. Sci.*, **12**, 206 (2019).
47. A. Chiara, F. Giannici, C. Pipitone, A. Longo, C. Aliotta, M. Gambino, and A. Martorana, "Solid-solid interfaces in protonic ceramic devices: a critical review." *ACS Appl. Mater. Interfaces*, **12**, 55537 (2020).
48. C. Zhao, Y. Li, W. Zhang, Y. Zheng, X. Lou, B. Yu, J. Chen, Y. Chen, M. Liu, and J. Wang, "Heterointerface engineering for enhancing the electrochemical performance of solid oxide cells." *Energy Environ. Sci.*, **13**, 53 (2020).
49. S. W. Saeed, T. Norby, and T. S. Bjørheim, "First-principles analyses of nanoionic effects at oxide-oxide heterointerfaces for electrochemical applications." *J. Phys. Chem. C*, **124**, 14072 (2020).
50. S. W. Saeed, T. Norby, and T. S. Bjørheim, "Charge-carrier enrichment at $BaZrO_3/SrTiO_3$ interfaces." *J. Phys. Chem. C*, **123**, 20808 (2019).
51. A. Bard and L. Faulkner, *Electrochemical Methods: Fundamentals and Applications* (Wiley, New York) 2nd edition ed. (2000).
52. S. C. DeCaluwe, P. J. Weddle, H. Zhu, A. M. Colclasure, W. G. Bessler, G. S. Jackson, and R. J. Kee, "On the fundamental and practical aspects of modeling complex electrochemical kinetics and transport." *J. Electrochem. Soc.*, **165**, E637 (2018).
53. R. P. Buck and P. Vanýsek, "Interfacial potential differences at mixed conductor interfaces: nernst, Nernst–Donnan, Nernst distribution and generalizations." *J. Electroanal. Chem. Interfacial Electrochem.*, **292**, 73 (1990).
54. T. Pacześniak, K. Rydel-Ciszek, P. Chmielarz, M. Charczuk, and A. Sobkowiak, "Electrochemical reaction Gibbs energy: spontaneity in electrochemical cells." *J. Chem. Educ.*, **95**, 1794 (2018).
55. R. J. Kee, H. Zhu, B. W. Hildenbrand, E. Vøllestad, M. D. Sanders, and R. P. O'Hayre, "Modeling the steady-state and transient response of polarized and non-polarized proton-conducting doped-perovskite membranes." *J. Electrochem. Soc.*, **160**, F290 (2013).
56. H. Shimada, Y. Yamaguchi, H. Sumi, and Y. Mizutani, "Enhanced $La_{0.6}Sr_{0.4}Co_{0.2}Fe_{0.8}O_{3-\delta}$-based cathode performance by modification of $BaZr_{0.1}Ce_{0.7}Y_{0.1}Yb_{0.1}O_{3-\delta}$ electrolyte surface in protonic ceramic fuel cells." *Ceram. Int.*, **47**, 16358 (2021).
57. S. Sun and Z. Cheng, "Electrochemical behaviors for Ag, LSCF and BSCF as oxygen electrodes for proton conducting IT-SOFC." *J. Electrochem. Soc.*, **164**, F3104 (2017).
58. A. V. Kasyanova, I. A. Zvonareva, N. A. Tarasova, L. Bi, D. A. Medvedev, and Z. Shao, "Electrolyte materials for protonic ceramic electrochemical cells: main limitations and potential solutions." *Mater. Reports Energy*, **2**, 100158 (2022).
59. T. Somekawa, Y. Matsuzaki, Y. Tachikawa, H. Matsumoto, S. Taniguchi, and K. Sasaki, "Physicochemical properties of proton-conductive $Ba(Zr_{0.1}Ce_{0.7}Y_{0.1}Yb_{0.1})O_{3-\delta}$ solid electrolyte in terms of electrochemical performance of solid oxide fuel cells." *Int. J. Hydrogen Energy*, **41**, 17539 (2016).
60. H. Zhu, S. Ricote, W. G. Coors, and R. J . Kee, "Interpreting equilibrium-conductivity and conductivity-relaxation measurements to establish thermodynamic and transport properties for multiple charged defect conducting ceramics." *Faraday Discuss*, **182**, 49 (2015).
61. T. He, K. D. Kreuer, Y. M. Baikov, and J. Maier, "Impedance spectroscopic study of thermodynamics and kinetics of a Gd-doped $BaCeO_3$ single crystal." *Solid State Ionics*, **95**, 301 (1997).
62. B. Guan, H. Tian, Y. N. Picard, J. Liu, H. W. Abernathy, T. Kalapos, L. Zhou, X. Li, W. L, and X. Liu, "Unraveling the conundrum of electronic leakage in protonic ceramic cells: operation-specific insights and rational design strategies." *J. Power Sources*, **604**, 234454 (2024).
63. N. Bonanos, "Oxide-based protonic conductors: point defects and transport properties." *Solid State Ionics*, **145**, 265 (2001).
64. R. Merkle, M. F. Hoedl, G. Raimondi, R. Zohourian, and J. Maier, "Oxides with mixed protonic and electronic conductivity." *Annu. Rev. Mater. Res.*, **51**, 461 (2021).
65. R. Merkle and J. Maier, "The significance of defect chemistry for the rate of gas–solid reactions: three examples." *Topics in Catalysis*, **38**, 141 (2006).
66. G. W. Coffey, L. R. Pederson, and P. C. Rieke, "Competition between bulk and surface pathways in mixed ionic electronic conducting oxygen electrodes." *J. Electrochem. Soc.*, **150**, A1139 (2003).
67. C. O. Park, S. A. Akbar, and W. Weppner, "Ceramic electrolytes and electrochemical sensors." *J. Mater. Sci.*, **38**, 4639 (2003).
68. U. K. Chakraborty, "Reversible and irreversible potentials and an inaccuracy in popular models in the fuel cell literature." *Energies*, **11**, 1851 (2018).
69. W. G. Bessler, S. Gewies, and M. Vogler, "A new framework for physically based modeling of solid oxide fuel cells." *Electrochim. Acta*, **53**, 1782 (2007).
70. H. Zhu, R. J. Kee, V. M. Janardhanan, O. Deutschmann, and D. G. Goodwin, "Modeling elementary heterogeneous chemistry and electrochemistry in solid-oxide fuel cells." *J. Electrochem. Soc.*, **152**, A2427 (2005).

71. M. Liang, J. Kim, X. Xu, H. Sun, Y. Song, S. Jeon, T. H. Shin, Z. Shao, and W. Jung, "Electricity-to-ammonia interconversion in protonic ceramic cells: advances, challenges and perspectives." *Energy Environ. Sci.*, **18**, 3526 (2025).
72. F. Kosaka, T. Nakamura, and J. Otomo, "Electrochemical ammonia synthesis using mixed protonic-electronic conducting cathodes with exsolved ru-nanoparticles in proton conducting electrolysis cells." *J. Electrochem. Soc.*, **164**, F1323 (2017).
73. D. Chen, H. Wang, S. Zhang, M. O. Tade, Z. Shao, and H. Chen, "Multiscale model for solid oxide fuel cell with electrode containing mixed conducting material." *AIChE J*, **61**, 3786 (2015).
74. A. Cammarata and L. Mastropasqua, "Theoretical analysis of mixed open-circuit potential for high temperature electrochemical cells electrodes." *Front. Energy Res.*, **11**, 1 (2023).
75. L. An, T. S. Zhao, Z. H. Chai, L. Zeng, and P. Tan, "Modeling of the mixed potential in hydrogen peroxide-based fuel cells." *Int. J. Hydrogen Energy*, **39**, 7407 (2014).
76. T. Ritter, J. Zosel, and U. Guth, "Solid electrolyte gas sensors based on mixed potential principle–A review." *Sensors Actuators B Chem*, **382**, 133508 (2023).
77. D. del Olmo, M. Pavelka, and J. Kosek, "Open-circuit voltage comes from non-equilibrium thermodynamics." *J. Non-Equilibrium Thermodyn.*, **46**, 91 (2021).
78. L. Wehrle, A. Ashar, O. Deutschmann, and R. J. Braun, "Evaluating high power density, direct-ammonia SOFC stacks for decarbonizing heavy-duty transportation applications." *Appl. Energy*, **372**, 123646 (2024).
79. Y. Lin, R. Ran, Y. Guo, W. Zhou, R. Ca, J. Wang, and Z. Shao, "Proton-conducting fuel cells operating on hydrogen, ammonia and hydrazine at intermediate temperatures." *Int. J. Hydrogen Energy*, **35**, 2637 (2010).
80. H. Zhang et al., "An efficient and durable anode for ammonia protonic ceramic fuel cells." *Energy Environ. Sci.*, **15**, 287 (2022).
81. H. Zhu, C. Karakaya, and R. J. Kee, "Modeling ammonia-fueled co-flow dual-channel protonic-ceramic fuel cells." *Int. J. Green Energy*, **19**, 1568 (2022).
82. S. Appari, V. M. Janardhanan, S. Jayanti, L. Maier, S. Tischer, and O. Deutschmann, "Micro-kinetic modeling of NH_3 decomposition on Ni and its application to solid oxide fuel cells." *Chem. Eng. Sci.*, **66**, 5184 (2011).
83. S. Davari, C. Cárdenas, M. Hettel, P. Lott, S. Tischer, S. Angeli, and O. Deutschmann, "Spatially resolvedmeasurements in a stagnation-flow ractor: kinetics of catalytic NH_3 decomposition." *Chemie Ing. Tech.*, **96**, 1735 (2024).
84. T. Hibino and K. Kobayashi, "Mixed potential response for hydrocarbons in a proton-conductive electrochemical cell operated at room temperature." *J. Electrochem. Soc.*, **161**, H326 (2014).
85. M. Yan, R. Arsyad, N. A. P. Namari, H. Suzuki, and K. Takeyasu, "Mixed-potential-driven catalysis in glucose oxidation." *ChemCatChem*, **16**, e202400322 (2024).
86. M. Yan, N. A. P. Namari, J. Nakamura, and K. Takeyasu, "Theoretical framework for mixed-potential-driven catalysis." *Commun. Chem.*, **7**, 69 (2024).
87. T. Ritter, G. Hagen, J. Lattus, and R. Moos, "Solid state mixed-potential sensors as direct conversion sensors for automotive catalysts." *Sensors Actuators B Chem*, **255**, 3025 (2018).
88. G. Hagen, K. Burger, S. Wiegärtner, D. Schönauer-Kamin, and R. Moos, "A mixed potential based sensor that measures directly catalyst conversion—A novel approach for catalyst on-board diagnostics." *Sensors Actuators B Chem*, **217**, 158 (2015).
89. S. C. DeCaluwe, P. J. Weddle, H. Zhu, A. M. Colclasure, W. G. Bessler, G. S. Jackson, and R. J. Kee, "On the fundamental and practical aspects of modeling complex electrochemical kinetics and transport." *J. Electrochem. Soc.*, **165**, E637 (2018).
90. A. M. Colclasure, K. A. Smith, and R. J. Kee, "Modeling detailed chemistry and transport for solid-electrolyte-interface (sei) films in li–ion batteries." *Electrochimica Acta*, **58**, 33 (2011).
91. V. Menon, V. M. Janardhanan, and O. Deutschmann, "A mathematical model to analyze solid oxide electrolyzer cells (SOECs) for hydrogen production." *Chem. Eng. Sci.*, **110**, 83 (2014).
92. A. Banerjee, Y. Wang, J. Diercks, and O. Deutschmann, "Hierarchical modeling of solid oxide cells and stacks producing syngas via H_2O/CO_2 co-electrolysis for industrial applications." *Applied Energy*, **230**, 996 (2018).
93. V. Menon, Q. Fu, V. M. Janardhanan, and O. Deutschmann, "A model-based understanding of solid-oxide electrolysis cells (SOECs) for syngas production by H_2O/CO_2 co-electrolysis." *Journal of Power Sources*, **274**, 768 (2015).
94. C. Wagner, "Beitrag zur Theorie des Anlaufvorgangs." *Zeitschrift für Phys. Chemie*, **21B**, 25 (1933).
95. J. R. Seidenberg, A. Mitsos, and D. Bongartz, "Interpreting concentration and activation overpotentials in electrochemical systems: A critical discussion." *J. Electrochem. Soc.*, **172**, 043506 (2025).